PLASMA TRANSPORT ACROSS THE HELIOPAUSE

H. J. FAHR, W. NEUTSCH

Institut für Astrophysik und Extraterrestrische Forschung, Universität Bonn, F.R.G.

S. GRZEDZIELSKI, W. MACEK, and R. RATKIEWICZ-LANDOWSKA

Space Research Centre, Polish Academy of Sciences, Warsaw, Poland

(Received 7 November, 1985)

Abstract. Existing heliopause models are critically rediscussed under the new aspect of possible plasma mixing between the solar wind and the ambient ionized component of the local interstellar medium (LISM). Based on current kinetic plasma theories, effective diffusion rates across the heliopause are evaluated for several models with turbulence caused by electrostatic or electromagnetic interactions that could be envisaged in this context. Some specific cases that may lead to high diffusion rates are investigated, especially in regard to their LISM magnetic field dependence.

For weak fields (less than 10^{-7} G), macroscopic hydrodynamic instabilities, such as of Rayleigh–Taylor or Kelvin–Helmholtz-types, can be excited. The resulting plasma mixing rates at the heliopause may amount to 20–30% of the impinging mass flow.

Recently, an unconventional new approach to the problem for the case of tangential magnetic fields at the heliopause was published in which a continuous change of the plasma properties within an extended boundary layer is described by a complete set of two-fluid plasma equations including a hybrid MHD-formulation of wave-particle interaction effects. If a neutral sheet is assumed to exist within the boundary layer, the magnetic field direction is proven to be constant for a plane-parallel geometry. Considering the electric fields and currents in the layer, an interesting relationship between the field-reconnection probability and the electric conductivity can be derived, permitting a quantitative determination of either of these quantities.

An actual value for the electrical conductivity is derived here on the basis of electron distribution functions given by a superposition of Maxwellians with different temperatures. Using two-stream instability theory and retaining only the most unstable modes, an exact solution for the density, velocity, and magnetic and electric fields can be obtained. The electrical conductivity is then shown to be six orders of magnitude lower than calculated by conventional formulas. Interestingly, this leads to an acceptable value of 0.1 for the reconnection coefficient.

By analogy with the case of planetary magnetopauses, it is shown here for LISM magnetic fields of the order of 10^{-6} G or larger that field reconnection processes may also play an important role for the plasma mixing at the heliopause. The resulting plasma mixing rate is estimated to amount to an average value of 10% of the incident mass flow. It is suggested here that the dependence of the cosmic-ray penetration into the heliosphere on the distribution of reconnecting areas at the heliopause may provide a means of deriving the strength and orientation of the LISM field.

A series of observational implications for the expected plasma mixing at the heliopause is discussed in the last part of the paper. In particular, consequences are discussed for the generation of radio noise at the heliopause, for the penetration of LISM neutrals into the heliosphere, for the propagation of cosmic rays towards the inner part of the solar system and for convective electric field mergings into the heliosphere during the course of the solar cycle, depending on the solar cycle variations. With concern to a recent detection of electrostatic plasma waves by plasma receivers on Voyagers 1 and 2, we come to an interesting alternate explanation: the *heliopause*, rather than the *heliospheric shock front*, could be responsible for the generation of these waves.

Table of Contents

Space Science Reviews **43** (1986) 329–381.

1. Introduction to the Problem

It has been known for quite a long time that at large solar distances the expanding solar wind is influenced by the counterstreaming of the interstellar plasma. This interaction of two highly conducting, magnetized plasmas was thought up to now to occur under MHD rather than kinetic conditions. No mutual penetration or plasma mixing of the two MHD-fluids was considered in a first-order treatment of the stationary case of the resulting interaction scenario. However, bringing to mind the leakage through the plasma discontinuity surfaces that are so often encountered both in laboratory and space plasma physics, we think it to be time to rediscuss critically the picture that is underlying this approach, especially the neglect of plasma transport effects.

1.1. The Heliopause as a Tangential Discontinuity

In the earlier approaches, it is assumed that a separatrix is formed, i.e., a curved boundary surface around the solar plasma source, where the two contacting fluids are kept separated from one another. Since the heliosphere is terminated by this boundary surface, the latter is called the heliopause. In the standard MHD notation, the heliopause is a plasma tangential discontinuity, as treated at length by Landau and Lifshitz (1963). The theoretical modelling of the 3-dimensional configuration of the heliopause in full generality is a very complicated problem that has not yet been solved. Solutions exist in the literature only for strongly simplified conditions.

First attempts to model the heliopause were undertaken by Parker (1963). As argued there, the heliopause results as a pressure equilibrium surface between the inner solar wind and the outer interstellar plasma. Parker investigated two standard approaches to

this problem, namely the heliopause as a result of (1) pure magnetic field confinement, and (2) pure plasma confinement.

(1) In the field-plasma case, Parker uses a magnetic field potential for a current-free interstellar space that surrounds a diamagnetic plasma cavity. The heliopause configuration was determined (Figure 1(b)) by selection of that specific field line which enables a stationary outflow of the solar plasma via two diametrically opposite outflow channels into interstellar space with pressure equilibrium across the line.

(2) A similar condition was established in an alternative model by Parker (1963) in which the confinement of the solar plasma cavity by an unmagnetized interstellar plasma flow was considered. The vector fields for the external and internal plasma flows are generated from a specific stream function potential which is a superposition of two potentials, one representing the outflow from a plasma point source, the other a homogeneous and unidirectional flow. Since the model is treating an incompressible fluid, the condition of pressure equilibrium is fulfilled everywhere and the separatrix thus is found by taking account of the strength of the solar plasma source which defines the stationary outflow of solar plasma into interstellar space (Figure 1(a)). In both cases, no plasma diffusion across the astropause was considered. Thus the continuity of the

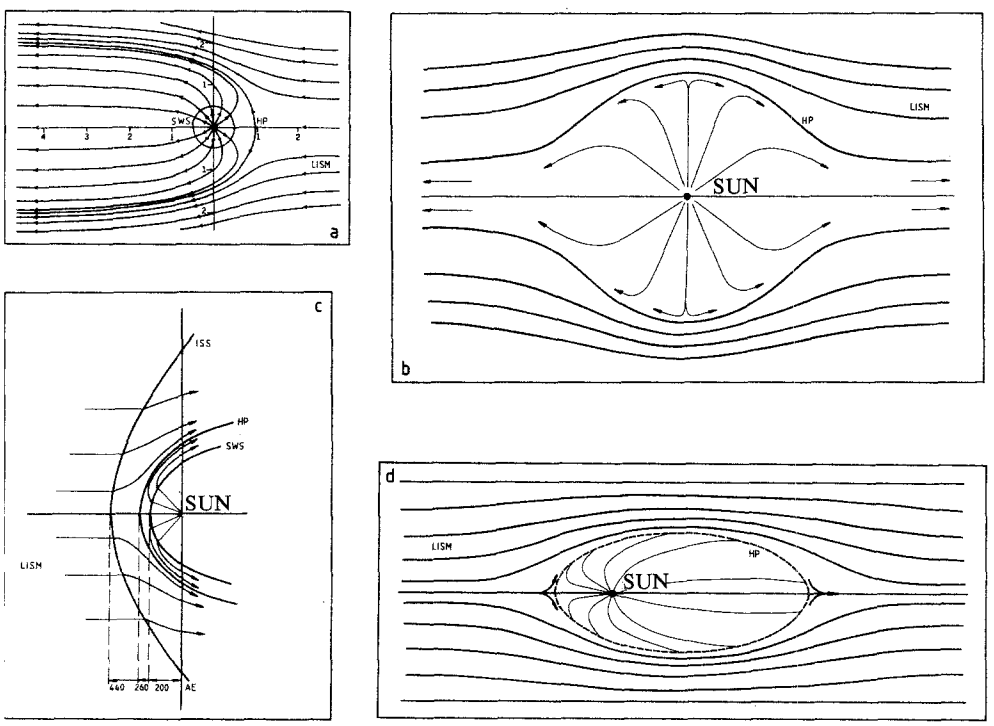

Fig. 1. Standard models of the heliospheric interface: (1a) Plasma-plasma interface for subsonic LISM flows according to Parker (1963). (1b) Field-plasma interface according to Parker (1963). (1c) Plasma-plasma interface for supersonic LISM flow according to Baranov *et al.* (1979). (1d) Plasma-plasma interface model with inclusion of plasma diffusion across the heliopause according to Neutsch and Fahr (1983).

outflow within the channels that the astropause extrudes towards interstellar space is a reasonable demand. If, however, some plasma diffusion across the heliopause has to be expected, investigating the continuity of the outflow becomes more complicated.

(3) For instance, if there is a diffusive plasma outflow across the heliopause, a closed structure topologically equivalent to a sphere (genus 0 surface) can be expected for the boundary surface. This situation has been treated theoretically by Neutsch and Fahr (1983). They have approximated the heliopause by an ellipsoidal geometry and have consistently treated the pressure equilibrium problem for a magnetized plasma flow passing over this plasma cavity. In their theoretical model, a submagnetoacoustic approach of the interstellar plasma towards the heliospheric cavity was assumed. An example of the heliopause configuration to be expected under these conditions is given in Figure 1(d).

(4) The cases of a supersonic or super-magnetosonic approach of the interstellar plasma towards the heliospheric obstacle have been investigated as an alternative to the models mentioned above. Assuming that the interstellar plasma, like the solar plasma, can be treated as essentially unmagnetized media, Baranov *et al.* (1976, 1979) have given a model for the heliopause that results from supersonic counterstreaming of the Local Interstellar Medium (LISM) and solar wind plasma. In this model, the heliopause is hit by both plasma flows after passage of a shockfront on each side, the interstellar shockfront located outside, the heliospheric shockfront inside the heliopause. A comparison of the properties of this heliospheric interface model with those of the aforementioned subsonic models was given in Ripken and Fahr (1983).

(5) The model of Baranov *et al.* (1976, 1979) does not allow for an inclusion of magnetic fields since the consistent treatment of the resulting magnetic forces is beyond the framework of their approach. Nevertheless, to study the properties of a super-magnetosonic counterflow of two magnetized plasmas, Fahr *et al.* (1985) have made use of the so-called Newtonian approximation. They assume that a resulting pressure equilibrium surface can be found by looking for a surface geometry which permits the fulfillment of the pressure equilibrium condition with the unperturbed pressure tensors of the plasma flow. In this approximation, both plasma pressures and magnetic field pressures are taken into account. It is shown by these authors that the heliopause geometry under these conditions is strongly influenced by the angle between the peculiar motion of the solar system and the interstellar magnetic field direction.

In all of these models mentioned above under numbers (1) through (5), no plasma mixing, or plasma diffusion, across the heliopause was considered in a consistent manner. The model of Neutsch and Fahr (1983), though allowing for a plasma diffusion out of the heliopause, treats this unspecified plasma transport only globally rather than locally, and thereby justifies the closed structure of the heliopause, as was shown in Figure 1(d). In Figures 1(a) and (b), we show models for a plasma-plasma or a field-plasma interface in which one and two outflow channels, respectively, are produced in order to take care of the continuous flow of solar wind plasma material to infinity for the case when no plasma mixing takes place. Thus the channel dimensions were calculated in both cases as to guarantee the constancy of this flow.

In case 1a, where the interstellar plasma is denser than the solar wind, any plasma transport that might exist is likely to be directed into the heliosphere, so that in the heliospheric tail the total plasma flow is systematically increased in the downwind direction. Thus a steady increase of the diameter of this cylindrical heliospheric tail region would result from this inward transport across the heliopause. On the other hand, in the interface model shown in Figure 1(b) where the heliosphere is surrounded by a vacuum magnetic field rather than by a plasma, any diffusion that might occur would be oriented towards the interstellar side and thus would systematically reduce the total flow of solar material through the two outflow channels. This clearly would lead to a systematic shrinking of the cross-sectional dimensions of the two outflow channels, eventually leading to a complete dissolution of the tails.

In connection with any mass transport, energy transport across the heliopause boundary also has to be expected. The consequences of this cannot be predicted, not even globally, prior to a quantitative treatment. Plasma transport across the heliopause will also lead to an assimilation of the plasma properties, i.e., they will weaken the contrast between the interstellar and the solar side, and thus will widen the cross dimension of the boundary layer. In order to come to a more realistic picture of the heliospheric interface, it is, therefore, strongly advised to consider mechanisms that give rise to a plasma transport across the heliopause and to compare their relative efficiencies and consequences.

1.2. Possible mechanisms of plasma transport across the heliopause

In the MHD treatment referred to above, the heliopause is regarded as an ideal discontinuity surface with both the $\mathbf{v}$ and $\mathbf{B}$ fields (velocity and magnetic fields) parallel to the surface on each side (tangential discontinuity). Evidence accumulated in magnetospheric research suggests, however, that this 'discontinuity' should be at least several Larmor radii thick. In the case when fluid-type instabilities or plasma kinetic instabilities can grow fast enough to convert a non-negligible part of the 'free energy' into collective oscillations, the heliopause may rather resemble a diffuse boundary layer. The thickness of this layer may then become related more to the spatial scales of the most active unstable modes than to the Larmor radius.

In this section, we shall briefly discuss several possibilities of plasma diffusion or flow across the heliopause that in principle could result in partial mixing of the two originally separate plasmas. We shall make use of the theoretical approaches that are available at the present and that were mostly developed for laboratory plasma. However, we expect that the underlying physics should be similar. Some of the discussed possibilities then will be pursued in greater detail in Sections 1, 2, and 3, with emphasis on the specific peculiarities of the heliopause.

We adopt the following picture of the general context into which the properties of the heliopause have to fit. On the solar side (called side 1), we expect to have, whatever the detailed model may be, a shocked solar wind plasma. Its density is $n_1 \sim 10^{-3}$ cm^{-3} or less if the terminating shock is at a solar distance $r \gtrsim 100$ AU. The temperature of the

ionic component should be several hundred eV, if it is related to the bulk motion energy of the hypersonic solar wind.

The pressure in the vicinity of the stagnation point has to be high enough to counterbalance the flow of momentum $(p_2 + \rho_2 U_2^2)_\infty$ (ρ, mass density; p, pressure; U_2, bulk velocity) carried by the LISM plasma. On the other hand, lateral expansion of the shocked solar wind plasma from the region of the stagnation point towards the flanks is opposed (at large distances) only by the thermal pressure of the LISM plasma $(p_2)_\infty$. The resulting pressure difference between the compressed 'nose' region of the heliosphere, at the stagnation point, and the flanks is of the order of $(\rho_2 U_2^2)_\infty$ and should impart bulk velocities tangential to the heliopause of the order of the speed of sound, $U_1 \simeq 100$–200 km s^{-1}, to the shocked solar wind plasma. These values are, nota bene, also characteristic for the Baranov *et al.* (1979) model. On the other hand, one can expect on the interstellar side (side 2) a (perhaps slightly shocked) plasma of the density $n_2 \sim 10^{-1}$ cm^{-3} and the temperature ~ 2 eV, flowing around the heliosphere with speeds (in the solar frame) of the order of 10–20 km s^{-1}. The numerical values representing conditions on both sides of the heliopause are summarized in Table I. For reference we also give values of several plasma parameter.

TABLE I

Nominal values for the plasma parameters at the stagnation point

	Shocked solar wind (side 1)	Interstellar plasma (side 2)
$n_i = n_e$ (hydrogen plasma)	10^{-3} cm^{-3}	10^{-1} cm^{-3}
$k_B T_i = k_B T_e$	200 eV	2 eV
B	10^{-6} G[a]	10^{-6} G
β	16	16
$V_{T,i} = (k_B T_i/m_i)^{1/2}$	138 km s^{-1}	13.8 km s^{-1}
$V_{T,e} = (k_B T_e/m_e)^{1/2}$	5930 km s^{-1}	593 km s^{-1}
V_A	69 km s^{-1}	6.9 km s^{-1}
C_s	253 km s^{-1}	25.3 km s^{-1}
$r_{gi} = V_{T,i}/\omega_{gi}$	14400 km	1440 km
$r_{ge} = V_{T,e}/\omega_{ge}$	337 km	33.7 km
ω_{gi}	0.01 s^{-1}	0.01 s^{-1}
$\omega_{lh} = (\omega_{gi}\omega_{ge})^{1/2}$	0.41 s^{-1}	0.41 s^{-1}
ω_{ge}	17.6 s^{-1}	17.6 s^{-1}
ω_{pi}	41.6 s^{-1}	416 s^{-1}
ω_{pe}	1780 s^{-1}	17800 s^{-1}
ν_e	3×10^{-11} s^{-1}	3×10^{-6} s^{-1}
$\nu_{ch\text{-}ex}$[b]	6×10^{-9} s^{-1}	1×10^{-9} s^{-1}

[a] Parker's spiral field gives $B = 2.4 \times 10^{-7}$ G at $r = 200$ AU (Burlaga, 1984). If the termination solar wind shock is strong B could be increased by a factor $\simeq 4$.

[b] Per proton, for neutral hydrogen density = 0.1 at cm^{-3}.

1.2.1. *Diffusion Resulting from Hydrodynamical Instabilities*

The tangential discontinuity separating plasmas 1 and 2 may become Kelvin–Helmholtz unstable if the 'free energy' associated with the relative motion $\mathbf{U} = \mathbf{U}_2 - \mathbf{U}_1$ exceeds a given critical value to be derived from the Kelvin–Helmholtz instability criterion. Then hydrodynamical turbulent mixing of the two media can occur.

Turbulent transport at the saturation level across a shear layer of finite initial thickness Z separating two compressible media moving with relative (gliding) velocity $\mathbf{U}$ was recently investigated by Miura and Pritchett (1982) and Miura (1982, 1984). The case studied corresponds to MHD fluids with initially uniform density and uniform magnetic field $\mathbf{B}$ parallel to the shear layer. Despite this idealization, some information for the heliopause can be extracted from the reported results of nonlinear computer simulations of the Kelvin–Helmholtz instability. For the 'transverse configuration' ($\mathbf{U} \perp \mathbf{B}$), the growth time scale of the most unstable Kelvin–Helmholtz mode is of the order of $0.14Z/U$ for $U \simeq (C_s^2 + V_A^2)^{1/2}$ (C_s, sonic velocity; V_A, Alfvénic velocity). After a time of the order of $50Z/U$ (saturation regime), the thickness of the turbulent layer becomes $\sim 10Z$. One may identify this situation with regions at the flanks of the heliopause where $U \sim (C_s^2 + V_A^2)^{1/2}$ on the 'lighter' solar side (1) (whose velocity is more relevant for the instability) and assume $Z \sim Xr_{gi} \simeq X \times 10^3$ km (with $X \simeq 1$–10^2, Table I) for a typical field of $B = 1 \times 10^{-6}$ G. Then, as the simulations indicate, well-developed vortices set in with a velocity component U_Z (perpendicular to the initial boundary, cf. Figure 2) of the order of up to 0.25U, which could correspond to some 20 km s^{-1} of cross-heliopause random velocity. These vortices should develop on an extremely short time-scale: $[50 \times X \times 10^3 \text{ km}/20 \text{ km s}^{-1}] \sim 1 \text{ hr} \times X$.

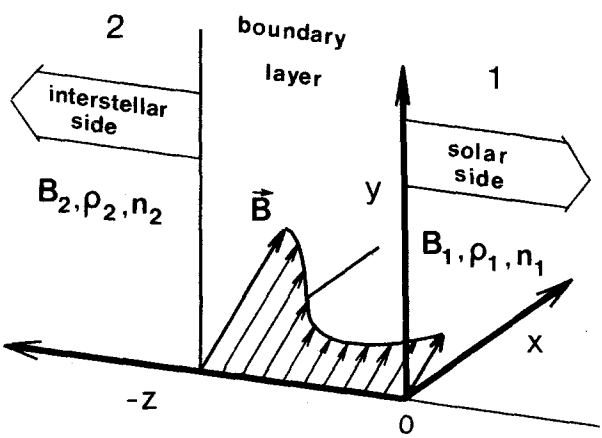

Fig. 2. Schematic view of the plane-parallel heliopause layer with tangential magnetic fields.

Even more pronounced circulation patterns may evolve in the 'parallel configuration' ($\mathbf{U} \parallel \mathbf{B}$) if the condition for the instability, $U > 2V_A$, is satisfied. This last inequality seems to be fulfilled over much of the frontal side of the heliopause if the field is weak

enough ($B = 3 \times 10^{-7}$ G) (Table I). Then, in the saturation stage (time $> 80Z/U$), U_Z becomes $\lesssim 0.3U$, which could mean $U_Z \simeq 40$ km s^{-1} for $\theta = 54°$ (for the Baranov *et al.* model, see Figure 1(c); θ denotes the angular distance from the upwind direction).

The computer simulations also allow Miura (1982) to calculate the effective anomalous viscosity. For the parallel configuration, it may attain or even exceed the value of the Bohm diffusion. In this context, it is worth noting that if the Bohm diffusion coefficient $D_B = c, k_B T/16eB$ (k_B, Boltzmann constant; T, temperature; e, elementary electric charge) were indeed representative for much of the front of the heliopause, then the thickness of the mixed layer should be of the order of $(D_B \tau)^{1/2}$, and if we take here as the relevant time-scale $\tau = \tau_F$, the flow time-scale of the LISM plasma, i.e., $\tau_F = \int_{s(\theta=0)}^{s(\theta)} ds/U_2 \simeq 10^{10}$ s for $\theta = 50°$, the thickness of the mixing layer becomes $10^{-2} - 10^{-1}$ AU for $B = 1 \times 10^{-6}$ G, depending on the assumed temperature.

Another inference of possible importance for the understanding of the conditions at the heliopause is the result found by Miura and Pritchett (1982) that the Kelvin–Helmholtz instability may fail to develop if U significantly exceeds the speed of sound or the speed of the fast magnetosonic wave. The analysis by Miura and Pritchett shows that the shear layer is no longer unstable in either the transverse configuration for $U > 2(C_s^2 + V_A^2)^{1/2}$ or in the parallel configuration for $U > 2C_s$. That might indicate that the heliopause becomes stable at large θ when U increases due to the fast flow of the shocked solar wind. However, that conclusion might be questioned in the case of the heliopause for the following reasons. First, as noted by Miura and Pritchett, the above limitations to the growth of unstable modes are relaxed for obliquely propagating modes. Second, the heliopause, being an 'open' layer, may not be well-represented by the assumptions underlying their analysis. In particular, there is no *a priori* reason for the expectation (as was assumed) that no energy in the form of MHD waves can be radiated away from the turbulent layer, i.e., that all unstable modes have to be evanescent at large distances. Most probably, the layer would still be unstable, although the growth time-scale could be longer.

The application of the above results to the heliopause may be somewhat doubtful in view of the large density gradient that is likely to exist. However, a large density jump combined with favourably-oriented acceleration may help destabilize the boundary by Rayleigh–Taylor instability, as is discussed in Section 2.

1.2.2. *Particle Diffusion Resulting from 'Anomalous' Transport Coefficients*

We shall assume the heliopause to be a flat layer of width $Z = Xr_{gi}$ with a diffusion coefficient $D = c^2/(4\pi\sigma)$. The 'anomalous' conductivity $\sigma = ne^2/(m_e \nu_{\text{eff}})$ results from the effective 'anomalous' collision frequency ν_{eff}. The characteristic diffusion time is then $\tau_D = Z^2/D = (Z\omega_{pe}/c)^2 \nu_{\text{eff}}^{-1}$ (ω_p, plasma frequency; m, mass; subscripts e and i stand for electron and ion, respectively; c, velocity of light) and the effective speed U_Z with which the plasma crosses the layer (which here is called U_D because of its diffusive nature)

$$\frac{U_D}{V_A} = \frac{r_{gi}}{Z} \frac{\nu_{\text{eff}}}{\omega_{pe}} \frac{c}{V_{T_i e}} \left(\frac{T_e}{T_i}\right)^{1/2} . \tag{1.1}$$

Here V_T is the thermal velocity. For convenience, we normalize the speed U_D with the local Alfvénic velocity V_A. As a reference value, one can take the speed U_D calculated for the classical cross-field diffusion coefficient $D_\perp = (m_e/m_i) r_{gi}^2 \nu_e$ (r_g, gyroradius). With the data from Table I, one then obtains $U_D/V_A = 2 \times 10^{-8}$.

As the magnetic fields on both sides are physically unrelated, the jump of the field across the layer is $\Delta B/Z \sim B/Z$. The current sheet supporting this jump corresponds to electrons in the layer drifting in the x, y-plane (see Figure 2), relative to the ions with speeds of the order of

$$u_d \simeq \frac{c}{4\pi} \frac{B}{enZ} \simeq \left(\frac{\omega_{lh}}{\omega_{pe}}\right)^2 \left(\frac{c}{V_{T,e}}\right)^2 \left(\frac{m_i}{m_e}\right)^{1/2} \left(\frac{T_e}{T_i}\right)^{1/2} \frac{r_{gi}}{Z} V_{T,e}, \tag{1.2}$$

ω_{lh} is the lower hybrid frequency. We shall first estimate U_D/V_A for turbulence excited by such electron drifts, assuming for the sake of simplicity that there are no gradients inside the layer.

The drift velocity u_d turns out to be small even for $Z \simeq r_{gi}$. For values from Table I, one obtains in this case $u_d \simeq 3$ km s^{-1}. This means that the threshold for the excitation of Buneman instability $u_d > V_{T,e}$ is not exceeded. Also, ion-sound instability seems to be improbable for two reasons. First, instead of $T_e \gg T_i$, one can rather expect $T_i > T_e$, as is usually the case in the shocked magnetosheath and in the magnetopause boundary layer. Second, the threshold condition $u_d > V_S$ can hardly be satisfied (cf. Table I). Therefore, the above-mentioned types of turbulence should not contribute to ν_{eff}.

There are, however, several instabilities that might develop for $T_i \simeq T_e$. The Bernstein-type mode may become unstable for wavelengths short enough to bring the electron cyclotron frequency ω_{ge} (Doppler shifted by u_d/k) (k, wave number) into resonance with the thermal motions of the ions. Galeev and Sagdeev (1984) give for the saturation stage in the nonlinear regime

$$\nu_{\text{eff}} \simeq 0.02 \frac{(u_d/V_{T,e})^3 \omega_{ge}}{1 + (\omega_{ge}/\omega_{pe})^2 (V_{T,e}/u_d)^2}. \tag{1.3}$$

Here ω_g is the gyrofrequency. From this, one can formally calculate D and U_D/V_A. In all following numerical estimates, we shall assume the width of the layer to be $Z = 15 r_{gi}$ ($X = 15$) as for the terrestrial magnetosphere (Cowley, 1982; Galeev, 1983) and also $kT_i \simeq 2$ eV, corresponding to the external, dense plasma ('heliosheath'). For $B = 1 \times 10^{-6}$ G, one then obtains for values from Table I and for $X \gg 1$, when the second term in the denominator in the right-hand side of Equation (1.3) becomes dominant,

$$\frac{U_D}{V_A} = 0.02 \frac{\omega_{pe}}{\omega_{ge}} \left(\frac{\omega_{lh}}{\omega_{pe}}\right)^{10} \left(\frac{c}{V_{T,e}}\right)^{11} \left(\frac{m_i}{m_e}\right)^{5/2} \left(\frac{T_e}{T_i}\right)^3 X^{-6} \simeq 10^{-14}. \tag{1.4}$$

Another instability possible for $T_i \simeq T_e$ and with a low threshold for excitation is the instability of the electrostatic modes on the lower hybrid frequency ω_{lh} with wave vectors perpendicular to the magnetic field. The authors quoted above give for the nonlinear

regime

$$\nu_{\text{eff}} \simeq \omega_{ge} u_d / V_{T,e}, \tag{1.5}$$

which leads to

$$\frac{U_D}{V_A} = \frac{\omega_{ge}}{\omega_{pe}} \left(\frac{\omega_{lh}}{\omega_{pe}}\right)^2 \left(\frac{c}{V_{T,e}}\right)^3 \left(\frac{m_i}{m_e}\right)^{1/2} \frac{T_e}{T_i} X^{-2} \simeq 10^{-5}. \tag{1.6}$$

In a realistic situation, however, density and temperature gradients should exist in the layer. The turbulence can then be due to unstable drift waves associated with the diamagnetic currents. For a low ratio β of the plasma pressure and the magnetic pressure ($\beta \ll 1$, this requires $B > 3 \times 10^{-6}$ G, cf. Table I), the instability can be enhanced by reverse gradients of density and temperature (as was discussed by Gladd and Horton, 1973) that should characterize the heliopause. The onset of turbulence also depends on the shear of the magnetic field in the layer. In the numerical estimates it will be assumed that $B = 1 \times 10^{-5}$ G to satisfy the condition $\beta \ll 1$ or $\beta < 1$. We shall also assume that the characteristic length scale of shear is $L_s \sim Z$. In the quasi-linear limit and for the Coulomb collision frequency exceeding the mean turbulent frequency ($\nu_e > \nu_*$) Liu *et al.* (1972) estimate the diffusion coefficient to be $D = V_{T,i} r_{gi} (m_e/m_i)^{1/2} (T_e/T_i)^2 X^{-1}$ which gives

$$\frac{U_D}{V_A} = \frac{\omega_{pe}}{\omega_{ge}} \frac{V_{T,e}}{c} \left(\frac{m_e}{m_i}\right)^{1/2} \left(\frac{T_e}{T_i}\right)^{3/2} X^{-2} \simeq 10^{-5}. \tag{1.7}$$

In the case of nonlinear saturation, Horton (1984) gives

$$D = V_{T,i} r_{gi} \left(\frac{m_e}{m_i}\right)^{1/2} \beta^{-1/2} \left(\frac{T_e}{T_i}\right)^{3/2} X^{-1}$$

and one obtains (for $\beta \sim 0.1$)

$$\frac{U_D}{V_A} = \frac{V_{T,e}}{c} \frac{m_e}{m_i} \beta^{-1} \frac{T_e}{T_i} X^{-2} \simeq 10^{-7}. \tag{1.8}$$

Faster diffusion may be suggested in view of the so-called convective cells connected with the parametric decay of the drift waves. The diffusion coefficient quoted by Horton (1984) is

$$D = V_{T,i} r_{gi} \left(\frac{m_e}{m_i}\right)^{1/4} \beta^{1/4} \frac{T_e}{T_i} \left(\frac{L_s}{Z}\right)^{1/2} X^{-1}, \tag{1.9}$$

which yields

$$\frac{U_D}{V_A} = \frac{\omega_{pe}}{\omega_{ge}} \frac{V_{T,e}}{c} \left(\frac{m_e}{m_i}\right)^{1/4} \beta^{1/4} \left(\frac{T_e}{T_i}\right)^{1/2} \left(\frac{L_s}{Z}\right)^{1/2} X^{-2} \simeq 10^{-4}$$

(assuming $\beta \sim 0.1$, $L_s \sim Z$).

On the other hand, when the plasma pressure is no longer small ($\beta \gtrsim 1$), the modes with a strong magnetic component become important. Such a situation seems to be typical in cases when reconnection of the magnetic lines of force accompanied by strong Ohmic dissipation occurs in small localized regions of a collisionless plasma. Galeev (1983) gives the effective collision frequency in a weak plasma turbulence approximation for such a localized region in which reconnection is driven by the lower hybrid drift instability. He finds for plasma with $\beta \sim 1$ (hereunder we shall assume $B = 3 \times 10^{-6}$ G) $\nu_{\text{eff}} = \frac{1}{8}\omega_{lh}(T_i/T_e)^2 X^{-3}$, which in turn yields

$$\frac{U_D}{V_A} = \frac{1}{8}\frac{\omega_{lh}}{\omega_{pe}}\frac{c}{V_{T,e}}\left(\frac{T_i}{T_e}\right)^{3/2} X^{-4} \simeq 10^{-7}. \tag{1.10}$$

Galeev (1983) also quotes another result valid for collapsing lower-hybrid drift oscillations (thin current sheets). One then has $\nu_{\text{eff}} = \frac{1}{4}\omega_{lh}(T_i/T_e)X^{-2}$, which gives

$$\frac{U_D}{V_A} = \frac{1}{4}\frac{\omega_{lh}}{\omega_{pe}}\frac{c}{V_{T,e}}\left(\frac{T_i}{T_e}\right)^{1/2} X^{-3} \simeq 10^{-6}. \tag{1.11}$$

Much higher rates are achievable with the assumption that the reconnection is due to the tearing-mode instability. Galeev (1978) gives two estimates for the velocity of merging of fields in regions where the dissipation takes place. In the case of an infinite plasma slab when ion drift in the polarization electric field compensates for the diamagnetic drift

$$\frac{U_D}{V_A} = \left(\frac{\omega_{ge}}{\omega_{pe}}\right)^{3/5}\left(\frac{c}{V_{T,e}}\right)^{3/5}\left(\frac{m_e}{m_i}\right)^{3/10}\left(\frac{T_e}{T_i}\right)^{3/10} X^{-3/5} \simeq 0.03. \tag{1.12}$$

An extremely high rate is obtained in the case when the magnetic field lines are, at the ends, imbedded in a well-conducting medium and the polarization electric field is short-circuited. Then

$$\frac{U_D}{V_A} = \left(\frac{\omega_{ge}}{\omega_{pe}}\right)^{9/13}\left(\frac{c}{V_{T,e}}\right)^{9/13}\left(\frac{m_i}{m_e}\right)^{9/26}\left(\frac{T_e}{T_i}\right)^{9/26} X^{-9/13} \simeq 0.2. \tag{1.13}$$

However, one may wonder whether such a short-circuit really is established in the heliosphere.

This short account of theoretical estimates indicates that the expected 'anomalous' transport of plasma across the heliopause may vary by several orders of magnitude depending on the actual plasma state. We give in Section 3 a detailed solution corresponding to diffusion processes driven by the electrostatic turbulence in the layer as an example of a type of structure that could appear with a suggested kind of plasma turbulence.

Another possibility is to adopt a phenomenological approach, i.e., to infer the average transport properties basing this on a perceived analogy with other well-studied cases of plasma in space, without relying on a particular theoretical scheme. This approach is

discussed in Section 4, and the results suggest a moderately fast rate of transport when averaged over a large heliopause area. Although this does not imply a uniquely specified mechanism, we feel that in view of the general importance of reconnection processes in space plasma studies and taking account of the high transport speeds predicted theoretically in these cases (Equations 1.12 and 1.13), heliopause reconnection of magnetic fields may be one of the main causes of 'anomalous' transport across the heliopause. A complementary aspect that should be considered in this context is the electrostatic turbulence determining the electric conductivity (cf. Section 3).

If this conclusion were to be substantiated by further studies, then a relationship should exist between the direction of the external (LISM) magnetic field and the rate of plasma transport across a given sector of the frontal heliopause (cf. Section 4.2). This may provide a means to infer the direction of the local interstellar magnetic field (cf. Section 5.1).

2. Mixing Due to Hydrodynamical Instabilities

The aim of this section is to discuss the possibility of plasma mixing due to hydrodynamical instabilities at the interface between the heliospheric and the interstellar plasmas. In the context of presently considered models of the boundary layers (cf. Section 1), two very simple hydrodynamical instabilities are worth being taken into account:

(1) Rayleigh–Taylor instability may appear if there is a large density jump combined with acceleration/gravity.

(2) Kelvin–Helmholtz instability may easily develop if a substantial velocity shear exists.

Both types of instabilities may operate only when the stabilizing effect of possible magnetic fields stays weak enough.

Although there is at the present no direct observational evidence relating to the heliopause, there is a large number of indirect data that may serve as a useful guide to the conditions at the termination of the solar wind.

In general, to induce the Rayleigh–Taylor instability, two fluids of different densities have to come into contact under the condition of appropriately oriented gravity or acceleration forces. At heliopause distances, only the latter factor is worth considering: in fact, the acceleration may be due to large-scale variations of the dynamical pressure of the solar wind related to solar activity. One can expect shifts of the heliopause on a relatively short time-scale of a few years.

From the observational point of view, the in-ecliptic variations of the solar wind velocity and number density over the 11-year solar cycle are well-known and are summarized by (for instance) Crooker (1982). We also have evidence for long-term variations in the solar wind associated with streams and/or larger structures that propagate radially outward from the Sun. This is evident from the daily averages of Pioneer 10 and 11 data for speed, particle flux and proton temperature (Kayser *et al.*, 1984), magnetic field data (Smith and Barnes, 1982) and Helios and Voyager speed and pressure profiles (Burlaga *et al.*, 1983).

The local dispersion in each parameter tells us that high-speed streams may be observed even at large heliocentric distances up to 28 AU (Kayser *et al.*, 1984). The solar cycle variations can be seen, for instance, in Figure 3 (from Smith and Barnes, 1982). The figure shows the extent to which significant time variations are present. There is a reasonably close correspondence between the speed variations at 1 AU and at large distances (Pioneer 10 having reached 25 AU in 1982). The persistence of large-scale pressure fluctuations in the distant solar wind can also be seen when comparing the Helios 1 and Voyager 1 data. Large-amplitude compression waves form as a result of sweeping and coalescence of many small-scale features ('entrainment', cf. Burlaga *et al.*, 1983).

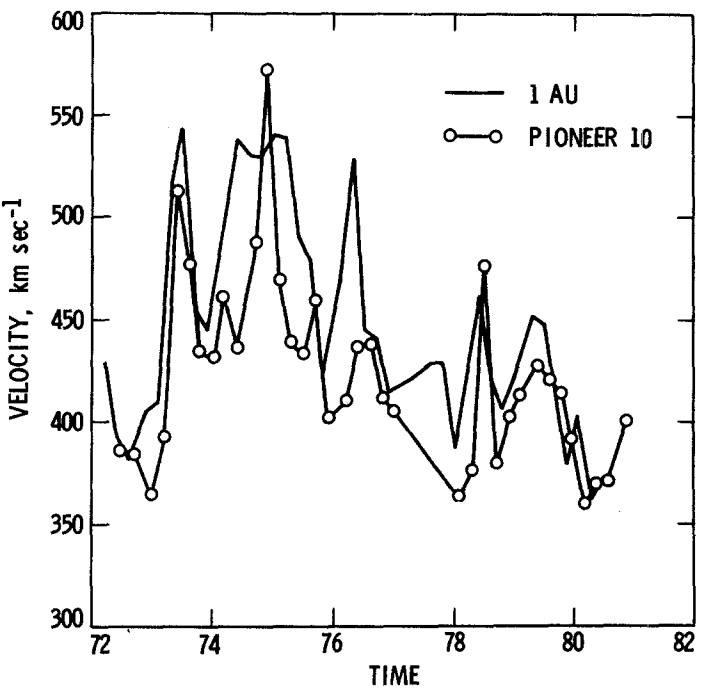

Fig. 3. Solar wind speed at 1 AU and as observed by Pioneer 10 (open circles connected by straight lines) are shown versus time in the solar cycle. The Pioneer 10 data represent average speeds measured during the flight of the spacecraft from 1 to 10 AU, however, corotated back to a corresponding time position at 1 AU. In general, the average speed at larger distances is correlated well with the solar wind speed at 1 AU. (Figure taken from Smith and Barnes, 1983.)

As for the last 11-year solar cycle (No. 20) from the data provided by Crooker (1982), one can calculate the time-dependence of the dynamical pressure of the solar wind $\rho_{SW} U_{SW}^2$ which is shown in Figure 4 (subscript 'SW' stands for solar wind conditions).

It is evident that, at least in the ecliptic plane, variations of the order of 20% are quite common, and larger changes are also possible (Vlasov, 1983). It is also clear that during the second half of the most recent 11-year cycle, $\rho_{SW} U_{SW}^2$ seems to be substantially

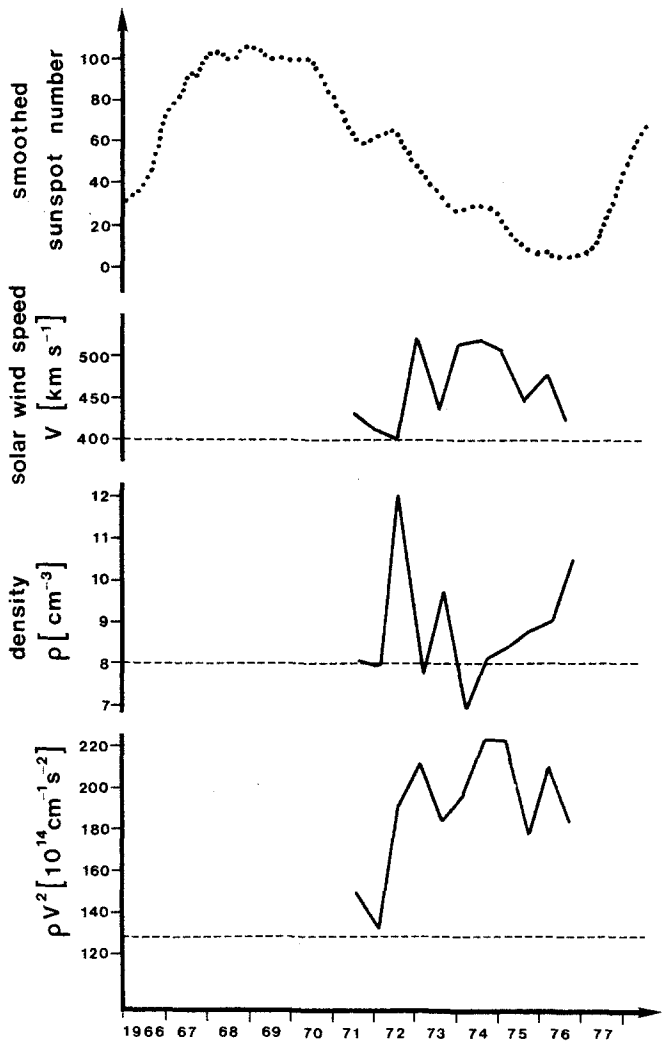

Fig. 4. Solar cycle variations of the solar wind particle density, velocity, and momentum flow are shown according to data given by Crooker *et al.* (1983).

larger than the dynamical pressure in the earlier years. The proper density contrast, which is also a necessary condition for the Rayleigh–Taylor instability, is fully consistent with the assumption of a strong terminating shock in the solar wind. This is the dominant feature in, for instance, the two-shock Baranov *et al.* (1979) model of the interaction between the solar wind and the interstellar ionized component (density contrast $\sim 10^2$). Since the compressed LISM plasma is much denser (heavier) than the shocked solar wind, the Rayleigh–Taylor instability may develop in the vicinity of the 'nose' of the heliosphere if the heliopause is subjected to an outward-directed acceleration. This should be the case when excess pressure is applied from the solar side.

At the same time, this type of model is characterized by a large jump of tangential velocities of the media separated by the heliopause. The velocity jump attains some ~ 100 km s^{-1} at an angle Θ, from the apex of the order of 30°. Therefore, the heliopause may become Kelvin–Helmholtz unstable at regions away from the 'nose'.

The Rayleigh–Taylor and Kelvin–Helmholtz instabilities were recently studied by Ratkiewicz-Landowska and Grzedzielski (1984) and Ratkiewicz-Landowska *et al.* (1985). The following combined Rayleigh–Taylor and Kelvin–Helmholtz instability criterion for locally incompressible media was used (case of uniform magnetic field **B**; Chandrasekhar, 1961):

$$\left(\omega + \left(\mathbf{k} \cdot \frac{\rho_1 \mathbf{U}_1 + \rho_2 \mathbf{U}_2}{\rho_1 + \rho_2}\right)\right)^2 =$$

$$= \frac{1}{\rho_1 + \rho_2}\left\{\frac{B^2}{2\pi} k^2 - \left[(\mathbf{ak})(\rho_2 - \rho_1) + \frac{(\rho_1 \cdot \rho_2)}{(\rho_1 + \rho_2)} \mathbf{U}^2 k^2\right]\right\}. \tag{2.1}$$

Here ω denotes the complex frequency and **k** is the wave vector. Instability corresponds to negative values of the right-hand side, when an imaginary part appears in ω.

In the above formula, **a** is the (constant) acceleration, $\rho_2(\rho_1)$ denotes the density of the dense (rarified) plasma and $\mathbf{U} = \mathbf{U}_2 - \mathbf{U}_1$ is the (tangential) velocity difference of the two media.

The motion of the boundary layer in the vicinity of the 'nose' of the heliopause was approximated by a one-dimensional, plane, compression wave generated by the momentaneous excess of the solar wind dynamical pressure over the average value in one solar cycle. In this approximation, the hot shocked solar wind behaves like an incompressible fluid since the time scale of a pressure wave to cross this thin layer is short compared with the solar cycle time-scale. On the other hand, the wide layer of comparatively cold LISM plasma behaves like a strongly compressible medium. Therefore, the shocked solar wind was simulated by a piston receding from the Sun with constant acceleration and pushing the cold (thus compressible) dense LISM plasma.

The resulting effective acceleration and maximum linear scales of Rayleigh–Taylor unstable nonmagnetic LISM plasma elements were calculated for several values of solar wind dynamical pressure variations. These corresponded to rather moderate solar cycle modulation of the average dynamical pressure (by up to 25%) (Hundhausen, 1979; Crooker, 1982; Vlasov, 1983).

Farther away from the nose towards the tail region, the Kelvin–Helmholtz instability associated with the compressed (dense) slow LISM flowing over the fast moving shocked solar wind plasma, takes over. The maximum rate of instability development will, of course, be obtained for vanishing magnetic field strength ($\mathbf{B} = 0$) or for a velocity **U** perpendicular to the direction of **B** on both sides of the interface. The results shown in Figure 6 correspond to the situation as described above. The rate of mass exchange across the heliopause depends on some characteristic time and length scales, τ_* and λ_*. τ_* is defined as the maximum time-scale allowed for the acceleration phase: here

$\frac{1}{4}$ of the solar cycle period was taken; λ_* is the longest possible associated wave length for which the heliopause is unstable and is calculated from the dispersion relation (2.1).

The quantities τ_* and λ_* enable one to estimate the maximum rate of mass exchange mixing through the heliopause in the following way. The flux of the interstellar gas through the heliopause per area $2\pi l \mathrm{d}s$ averaged over one solar cycle is equal to:

$$F_2 = \tfrac{1}{2} \times 2\pi l \,\mathrm{d}s \,\frac{\frac{1}{2}\lambda_*}{4\tau_*}\,\rho_2 \;=\; \tfrac{1}{16} \times 2\pi R \sin\Theta \,\mathrm{d}s \,\frac{\lambda_*}{\tau_*}\,\rho_2 \tag{2.2}$$

(l is the distance from the axis of symmetry (z-axis, Figure 5)). The corresponding mass flux in the reverse direction of the compressed solar wind is by analogy

$$F_1 = \tfrac{1}{16} \times 2\pi R \sin\Theta \,\mathrm{d}s \,\frac{\lambda_*}{\tau_*}\,\rho_1 \,. \tag{2.3}$$

In the above estimates, we assume that mixing is effective to a depth equal to $\frac{1}{2}\lambda_*$. This corresponds, for instance, to about 4 AU at the angular distance $\Theta = 54°$ from the apex is the forcing frequency for the Kelvin–Helmholtz instability is assumed to be as low as the solar cycle frequency. In conservative calculations, taking periods of at the

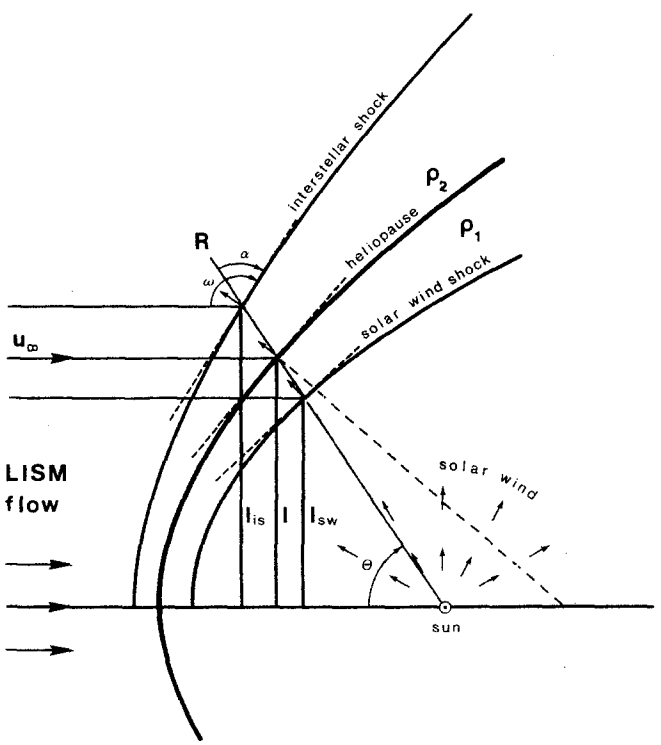

Fig. 5. Illustrative view of the heliopause configuration including inner heliospheric and outer interstellar shock as a definition of relevant quantities for calculations.

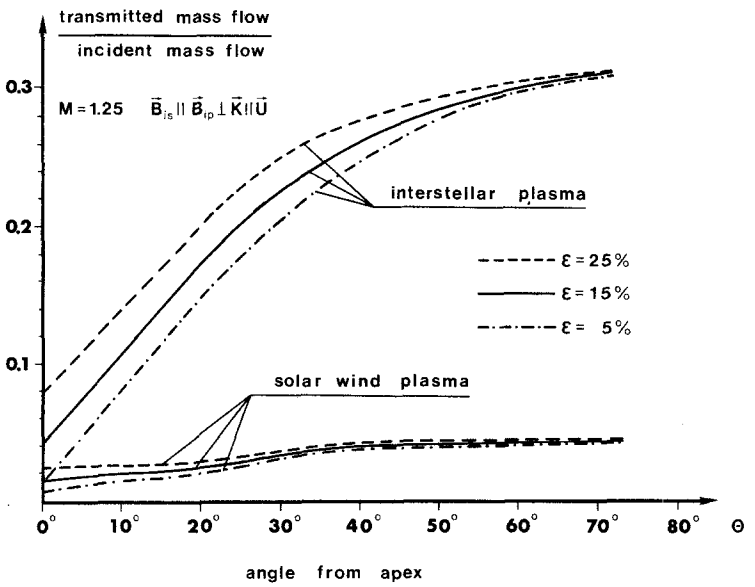

Fig. 6. Ratios between transmitted and incident LISM or solar wind plasma flows are shown as a function of the angle θ at which the heliopause is reached by these flows. Results are obtained taking into account simultaneously the effects of macroscopic Kelvin–Helmholtz and Rayleigh–Taylor turbulence. The parameter ε gives a measure for the relative amplitude of the solar wind pressure variation during one half of a solar cycle.

most $\frac{1}{4}$ of the solar cycle in order to make the Kelvin–Helmholtz waves marginally unstable, the mixing depth is decreased accordingly.

The relative mass flux (normalized by the incident flux) is then, correspondingly,

$$F_2 = \frac{1}{16}\left(\frac{R}{R_2}\right)^2 \frac{1}{\sin\omega_2} \frac{(\lambda_*/\tau_*)\rho_2}{(\rho_2 U_2)_\infty},$$

$$F_1 = \frac{1}{16}\left(\frac{R}{R_1}\right)^2 \frac{1}{\sin(\omega_1 - \Theta)} \frac{(\lambda_*/\tau_*)\rho_1}{\rho_{SW} U_{SW}}; \tag{2.4}$$

where $R, R_2, R_1, \omega_2, \omega_1, \rho_1, \rho_2, \lambda_*$, and ρ_{SW} are functions of Θ (cf. Figure 5). $(\rho_2 U_2)_\infty$ denotes the impinging mass flux of the LISM plasma, ρ_{SW} is the solar wind mass density prior to the shock transition,

$$\rho_{SW} = \rho_{SW}^E \left(\frac{R_E}{R_1}\right)^2, \tag{2.5}$$

(ρ_{SW}^E, R_E corresponding values at terrestrial orbit).

In the simplest treatment, assuming that

$$\left(\frac{R}{R_2}\right)^2 \frac{1}{\sin\omega_2} \sim 1 \quad \text{and} \quad \left(\frac{R}{R_1}\right)^2 \frac{1}{\sin(\omega_1 - \Theta)} \sim 1$$

(these are within 20% of the Baranov *et al.* model), the resulting relative mass exchange rates F_1 and F_2 are shown in Figure 6 (adopted from Ratkiewicz-Landowska and Grzedzielski, 1984) as functions of the polar angle Θ counted from the apex. The curves are parameterized by the relative amplitude ε of the modulation of the solar wind dynamical pressure around its average value. It is evident that the Kelvin–Helmholtz instability operating at the flanks may result in a substantial mass transport across the heliopause. The Rayleigh–Taylor instability in the vicinity of the 'nose' is of minor importance. However, even in that case, a few percent of the impinging flux of the interstellar gas may penetrate directly into the shocked solar wind.

3. Instability-Driven Plasma Transport

3.1. Importance of electrostatic instabilities

It has been emphasized (see, for instance, Landau and Lifshitz, 1963; Parker, 1979; Lee and Roederer, 1982) that the transition relations alone, formulated in terms of Poisson brackets of the relevant quantities for the continuity requirements at plasma contact discontinuities, do not allow for unique solutions. For instance, the question whether or not a specific form of a plasma-, energy-, and field-transport across the discontinuity surface exists is kept open and, in all practical cases, is still a matter of debate.

For a quantitative determination of these transports, the boundary conditions on both sides of the discontinuity and the internal structure of the transition layer have to be carefully considered. The problem of treating the continuous change of plasma properties within the boundary layer dates back to publications by Fejer (1964, 1965); Sen (1965); Lerche (1966); Parker (1967a, b); and Willis (1971), who considered the microstructure of a boundary layer that confines a magnetic field to a plasma flow. It was argued there that due to the single particle kinetics of gyrating ions and electrons, an electric charge separation is expected which, together with the plasma flow, should lead to electrical currents in the layer. Though Coulomb interactions clearly can be neglected, it has meanwhile been pointed out that the underlying assumptions of an independent motion of electrons and ions in the layer must be strongly questioned (Robertson *et al.*, 1981; Lee, 1982; Fahr and Neutsch, 1982a, b; Smith *et al.*, 1984; Smith, 1984). This is because strong electrostatic plasma waves are most likely to be excited and kept on a fairly high fluctuation level by the ion motions, and a rapid coupling of the electron distribution function to these fluctuating fields occurs. Couplings may also be due to ion acoustic and magnetosonic wave noise in the transition layers, especially since the plasma data given in Table I can be taken only as an orientation. This is caused by different ions counterstreaming fast enough from the interstellar and the solar side.

As was argued by Fahr and Neutsch (1982a, b) and later confirmed by more detailed calculations by Smith *et al.* (1984) and Smith (1984), electrostatic plasma oscillations are most relevant in this context. This is due to the fact that the characteristic growth periods for these oscillations caused by two-stream instability excitations in the plasma

layer turn out to be much shorter than the ion transit times and the ion and electron gyroperiods. This kind of instability could be excited under conditions involving two plasma flows penetrating each other or counterflowing ion jets maintained in the boundary layer. Therefore, the coupling to the electric fluctuation field is much stronger than the coupling to the stationary magnetic field **B**. Hence, ions and electrons do not feel this stationary field in a first-order approximation. Under such conditions, the numerical results of Davidson *et al.* (1969) concerning nonlinear plasma-wave coupling in the saturation mode show that a specific relation is established between the electron temperature T_e and the relative drift velocity U_z with respect to the ions which is given by

$$T_{ez} = \frac{m_e U_z^2}{2k_B}, \tag{3.1}$$

where k_B is the Boltzmann constant and the suffix 'z' indicates that this relation may be used for quantities evaluated for a specific coordinate axis z. m_e and m_i are the masses of electrons and ions, respectively.

As was shown by Fahr and Neutsch (1982a, b), this enables one to write the electron and ion pressure terms in a hybrid form of two-fluid plasma equations as pure functions of the mass density corresponding to a polytropic index $\kappa = -1$. The friction terms $\mathbf{R}_{e,i} = \mathbf{R}_{i,e}$ that enter the two-fluid plasma equations and describe the mutual momentum transfer between electrons and ions can also be evaluated on the basis of a plasma coupling to the saturated electrostatic wave field. It can be shown that they, too, are obtained as pure functions of ρ in the following form:

$$|\mathbf{R}_{e,i}| = |-\mathbf{R}_{i,e}| \frac{39.905(m_e/m_i)K^2(1/\rho)}{\sqrt{\frac{k_B T_0}{m_e} + \frac{K^2}{2\rho^2}}} \gamma_{\max} =$$

$$= \frac{A}{\rho}\left(\frac{k_B T_0}{m_e} + \frac{K^2}{2\rho^2}\right)^{-1/2}, \tag{3.2}$$

where $\gamma_{\max}$ is the maximum growth rate of electrostatic oscillations and K is the magnitude of the mass flow in the direction of the boundary surface normal.

Applying the two-fluid plasma equations given by Schlüter (1950) to a one-dimensional boundary layer (planar approximation; see illustration in Figure 2 and using Equations (3.1) and (3.2), Fahr and Neutsch obtain the following complete set of differential equations for the determination of the MHD properties of the boundary layer plasma:

$$KU_x' = 0, \tag{3.3}$$

$$KU_y' = 0, \tag{3.4}$$

$$KU_z' = -\frac{1}{4\pi}(B_y B_y' + B_x B_x') + \frac{1}{2}\left(1 + \frac{m_e}{m_i}\right)K^2 \frac{\rho'}{\rho^2}, \tag{3.5}$$

$$\frac{m_i m_e c^2}{4\pi e^2}\left(\frac{B'}{\rho}\right)' = B_y\,, \tag{3.6}$$

$$\frac{m_i m_e c^2}{4\pi e^2}\left(\frac{B'_x}{\rho}\right)' = B_x\,, \tag{3.7}$$

$$0 = E_z + \frac{1}{c}(U_x B_y - U_y B_x) + \frac{c}{4\pi nec}\,(B_y B'_y + B_x B'_x) -$$

$$- \frac{A}{en}\left(\frac{k_B T}{m_c}\,\rho^2 + \frac{K^2}{2}\right)^{-1/2}. \tag{3.8}$$

Here the primes mean derivatives with respect to the coordinate z, and the quantity A is explained in Equation (3.2).

Equations (3.13) *and* (3.14) *can then be integrated to yield*:

$$U_x = U_{x_{1,2}} = \text{const.}; \qquad U_y = U_{y_{1,2}} = \text{const.} \tag{3.9}$$

Two more integration constants can be immediately extracted from this set of equations:

$$K = \rho U_z = \rho_{1,2} U_{z_{1,2}} \tag{3.10}$$

and

$$G = \frac{B^2}{8\pi} + \frac{3}{2}\,\frac{K^2}{\rho} = \frac{B^2_{1,2}}{8\pi} + \frac{3}{2}\,\frac{K^2}{\rho_{1,2}}\,, \tag{3.11}$$

where U_z is the common plasma drift velocity in z-direction and where the suffixes '1' and '2' denote the boundary values on the solar side and the interstellar side, respectively.

From Equations (3.6) and (3.7) one can derive the validity of the following interesting relation:

$$B_x B''_y - B_y B''_x = (B_x B'_y - B_y B'_x)\,\frac{\rho'}{\rho}\,, \tag{3.12}$$

leading to the solution

$$W = (W/\rho)_0\,\rho\,, \tag{3.13}$$

with the Wronskian $W = B_x B'_y - B_y B'_x$, $(W/\rho)_0$ being a reference value at some place $z = z_0$.

If at some position z_0 within the layer the magnetic field vanishes (e.g., in the case of a neutral sheath!), it is clear that there also the quantity W_0 will attain the value 'zero', unless $\rho_0 = 0$. According to Equation (3.13), the Wronskian W should then vanish everywhere in the layer, implying a conservation of the direction of the magnetic field vector. This means that at least in this planar approximation for the boundary layer, no rotational discontinuity of the magnetic field would be permitted.

For the magnitude of the magnetic field, one then obtains the following second-order differential equation:

$$B'' - B' \frac{\rho'}{\rho} - g\rho B = 0\,, \tag{3.14}$$

where $g = 4\pi e^2/m_e m_i c^2$ is a constant. This equation can be integrated once by introducing a new variable $s = 3K^2/2G\rho$, which yields the following first-order differential equation:

$$B's = \frac{3}{2}\frac{K^2}{G}\sqrt{\left(\frac{B'}{\rho}\right)_1^2 - \frac{8\pi g F^2}{3K^2}(s^2 - s_1^2)}\,, \tag{3.15}$$

allowing a solution for z as a function of s in the form of an elliptic integral:

$$z - z_1 = \frac{2}{K}\sqrt{\frac{G}{3g}}\int_{s_1}^{s}\frac{s\,\mathrm{d}s}{\sqrt{4(s-\Gamma)(s+1)(s-1)}}\,, \tag{3.16}$$

where the quantity Γ has been introduced by

$$\Gamma^2 = \frac{3K^2\left(\frac{B'}{\rho}\right)_1^2}{8\pi g G^2} + s_1^2\,. \tag{3.17}$$

For numerical evaluation purposes it is recommended to change over to the Legendre–Jacobi form of the elliptic integrals (see Whittaker and Watson, 1927). With this reformulation of (3.16), one finally arrives at the following results:

$$s = \frac{1 - \Gamma \overset{*}{k}^2 \sin\phi}{1 - \overset{*}{k}^2 \sin^2\phi}\,, \tag{3.18}$$

$$z - z_1 = \frac{1}{K}\sqrt{\frac{2G\Gamma}{3g}}\left\{\overset{*}{F}(\phi, \overset{*}{k}) - 2\overset{*}{E}(\phi, \overset{*}{k}) + \frac{2\overset{*}{k}^2 \sin\phi\cos\phi}{\sqrt{1 - \overset{*}{k}^2\sin^2\phi}}\right\}, \tag{3.19}$$

$$\rho = \frac{3K^2}{2G}\frac{1 - \Gamma\overset{*}{k}^2\sin^2\phi}{1 - \overset{*}{k}^2\sin^2\phi}\,, \tag{3.20}$$

$$B = \sqrt{4\pi G\left(\frac{\Gamma^2 - 1}{\Gamma}\right)}\frac{\sin\phi}{\sqrt{1 - \overset{*}{k}^2\sin^2\phi}}\,. \tag{3.21}$$

Here $\overset{*}{k}$ has been set equal to $\sqrt{(\Gamma+1)/2\Gamma}$, $\overset{*}{F}(\phi, \overset{*}{k})$ and $\overset{*}{E}(\phi, \overset{*}{k})$ are elliptic integrals of the first and of the second order and ϕ is the independent variable.

For a discrete set of solutions $B(z)$, $U(z)$, $\rho(z)$ some problems now arise in connection with the boundary values needed on the interstellar and the solar sides. Specifically, the family parameter Γ requires a boundary value for the gradient of the magnetic field in

addition to the constants K and G. This numerical value may not be easily available. Thus without any specific knowledge concerning this gradient, the solutions (3.18) through (3.21) may be parametrized only with Γ.

Assuming that values for the density ρ and the magnetic field B are known on both sides of the layer, the integration constants K and G are defined by:

$$K^2 = \frac{1}{12\pi} \frac{B_2^2 - B_1^2}{(\rho_2 - \rho_1)} \rho_2 \rho_1 \tag{3.22}$$

and

$$G = \frac{B_2^2}{8\pi} + \frac{3}{2} \frac{K^2}{\rho_2}. \tag{3.23}$$

Whereas mass flow K and energy flow (KG) crossing over the layer can be fixed by these boundary values, the parameter Γ needs additional information about the field gradient on the solar side:

$$\Gamma^2 = \frac{3K^2}{4\rho_1 G^2} \left(3K^2 + \frac{B_1'^2}{2\pi g} \right). \tag{3.24}$$

To calculate concrete values for these constants we shall take for the interstellar side:

$$B_2 = 3 \times 10^{-6}\,\mathrm{G}; \qquad \rho_2 = m_i \times 10^{-2}\,\mathrm{cm}^{-3}.$$

At the solar side, we have to make an assumption for the location of the heliopause. Here we shall adopt $R_H = 250 R_E (1 R_E = 1\ \mathrm{AU})$. Assuming a decrease of ρ with solar distance proportional to $1/R^2$ in the supersonic solar wind regime, a 'strong shock' compression by a factor of 4 at the helioshock, and a nearly incompressible plasma behaviour in the subsonic region, we obtain

$$\rho_1 = 4 \times 5 m_i \left(\frac{R_E}{R_s} \right)^2 = 2 \times 10^{-3}\, m_i [\mathrm{g\,cm}^{-3}] \quad \text{for} \quad R_S = 100 R_E. \tag{3.25}$$

For the solar magnetic field, we shall adopt Parker's description for the azimuthal component of the Archimedean spiral field (Parker, 1958). At a heliopause point in the ecliptic at $250 R_E$ distance from the Sun we may thus calculate a field

$$B_1 = 4 B_{aE} (R_E / R_H) = 8 \times 10^{-7} [\mathrm{G}]; \qquad B_{aE} = 5 \times 10^{-5} [\mathrm{G}], \tag{3.26}$$

where B_{aE} means the azimuthal field component at $R = R_E$, and

$$B_1' = \left| \frac{\mathrm{d}B}{\mathrm{d}R} \right|_1 = -4 B_{aE} / R_E (R_E / R_H)^2 = 2 \times 10^{-22}\,\mathrm{G\,cm}^{-1}. \tag{3.27}$$

To estimate B_1', we have here simply assumed a continuation of the spherical expansion into the subsonic solar wind regime, with an inclusion of a field compression by a factor of 4 at the helioshock. Any more sophisticated model concerning the magnetic field

gradient B_1' at the heliopause would cause only a very minor change in Γ and K, as is confirmed by Equations (3.22) and (3.24).

With these boundary conditions, one obtains the following values for the relevant constants of the problem:

$$K^2 = 9.27 \times 10^{-40}\,[\mathrm{g\,cm^{-2}\,s^{-1}}]\,; \qquad G = 3.59 \times 10^{-13}\,[\mathrm{G \times G}]\,;$$

$$\Gamma = 1.0763\,.$$

A set of solutions for this set of parameters is shown in Figures 9, 10, 11. Furthermore, Figure 8 shows the variation of the total extent $Z = z_2 - z_1$ of the transition layer with the parameter Γ. It is evident that with Γ approaching 1, the extent Z increases towards infinity.

3.2. Relations between electrical conductivity, magnetic Reynolds number, and parameters K, Γ, G

Following arguments given by Parker (1979), we consider a boundary layer with some essentially planar geometry and a surface area of a magnitude L^2 (L being a characteristic dimension of the co-planar surface dimensions). Over the extent Z of the layer, a magnetic field with a co-planar orientation may change from $\mathbf{B}_2 = \mathbf{B}_0$ to $\mathbf{B}_1 = -\mathbf{B}_0$. The spatial change of the magnetic field vector is then connected with local electrical currents $\mathbf{j}$ according to

$$\nabla \times \mathbf{B} = \frac{4\pi}{c}\mathbf{j}\,. \tag{3.28}$$

Due to the planar geometry, we can neglect derivatives with respect to the planar space coordinates x, y. For $\mathbf{B}_0$ oriented in an x-direction one thus retains only

$$j_y = \frac{c}{4\pi}\frac{\mathrm{d}B_x}{\mathrm{d}z}, \tag{3.29}$$

which over the dimension Z of the layer has an average magnitude of

$$\langle j_y^2 \rangle = \left(\frac{c}{4\pi}\frac{2B_0}{Z}\right)^2. \tag{3.30}$$

The entire energy that is dissipated per unit of time in a volume ZL^2 of the layer, therefore, amounts to

$$\Delta^- \varepsilon = \frac{\langle j_y^2 \rangle}{\sigma}(ZL^2)\,, \tag{3.31}$$

where σ means the electrical conductivity.

In an equilibrium condition in connection with the flow velocity U_{z2}, an equivalent amount of energy thus has to be convected into the layer. The required energy flow

consists of a flow of kinetic energy, a flow of thermal enthalpy, and a flow of magnetic enthalpy, i.e., the Poynting vector flow. Through a surface area L^2, therefore, the following energy is convected per unit of time:

$$\Delta^+ \varepsilon = L^2 U_{z2} \left[\frac{B_2^2}{4\pi} + \rho_2 \left(\frac{U_{z2}^2}{2} + \frac{\kappa_i}{\kappa_i - 1} \frac{k_B T_i}{m_i} + \frac{\kappa_e}{\kappa_e - 1} \frac{k_B T_e}{m_i} \right) \right], \tag{3.32}$$

where κ_e and κ_i are the polytropic indices for electrons and ions. We assume thermal equilibrium between electrons and ions far off the layer. Furthermore, we adopt polytropic indices $\kappa_i = \kappa_e = \frac{5}{3}$. In view of the impeded heat conduction of electrons perpendicular to the magnetic field and by inspection of the results of the boundary solutions presented in Section 3.1, we realize that the convection velocity U_z always stays smaller than the local ion sound velocity $C_s^2 = \kappa_1 k_B (T_i + T_e)/m_i$. Thus one obtains with Equation (3.32)

$$\Delta^+ \varepsilon = L^2 U_{z2} [B_2^2/4\pi + \tfrac{35}{6} \rho_2 k_B T/m_i] , \tag{3.33}$$

which, together with $K = \rho_2 U_{z2}$, attains the form:

$$\Delta^+ \varepsilon = L^2 K [B_2^2/4\pi\rho_2 + \tfrac{35}{18}(3k_B T/m_i)] = L^2 K [V_{A2}^2 + \tfrac{35}{18} C_{s2}^2] , \tag{3.34}$$

where V_A and C_s are the Alfvén velocity and the plasma sound velocity, respectively. Now equating Equations (3.31) and (3.34) and then solving for the quantity K yields the following result:

$$K = \left(\frac{c^2}{\pi Z \sigma} \right) \rho_2 \frac{V_{A2}^2}{V_{A2}^2 + 2C_{s2}^2} , \tag{3.35}$$

where $\frac{35}{18}$ has been approximated by 2, which in view of the accuracy that is aimed for here seems adequate.

Finally, we arrive at the following expression:

$$K = \rho_2 V_{A2} \left(\frac{4}{R_M} \frac{V_{A2}^2}{V_{A2}^2 + 2C_{s2}^2} \right), \tag{3.36}$$

with the magnetic Reynolds number R_m given by:

$$R_m = \frac{4Z V_{A2}}{c^2} = \frac{V_{A2} Z}{\eta} , \tag{3.37}$$

where η means the electrical resistivity.

Calling to mind the meaning of the reconnection probability α given in papers by Sonnerup (1970) and Parker (1977), the following representation is found for this quantity:

$$\alpha = \frac{K}{\rho_2 V_{A2}} = \frac{4}{R_m} \frac{V_{A2}^2}{V_{A2}^2 + 2C_{s2}^2} . \tag{3.38}$$

In order to be evaluated, this representation requires as a necessary prerequisite a value for the appropriate electrical conductivity σ. In connection with this value, α can be calculated as a function of the boundary conditions with Equation (3.38) and the mass flow K can be fixed with Equation (3.36).

3.3. The Electrical Conductivity at the Heliopause

When applying Equation (3.31) to estimate the electrical energy dissipated in the boundary layer per unit of time due to some kind of 'Ohmic heating', use was made of the well-known electrical conductivity concept. Under 'classical', i.e., collision-dominated plasma conditions, this quantity is well explained and is simply given by (see for instance, Spitzer, 1956)

$$\sigma = \frac{e^2 n}{m \nu_c} = \frac{\omega_{pe}^2}{4\pi \nu_c}, \tag{3.39}$$

where ν_c is the average electron collision frequency for momentum transfer to the ions. For the specific case of the heliopause boundary layer plasma, the application of Equation (3.39) is inappropriate and unjustified since the motion of the electrons with respect to the ions in the presence of a static electric field E_0 is controlled by interactions with the electric fluctuation field $\mathbf{E}_1$ rather than by collisions. In this case, electrons subject to a field $\mathbf{E}_0$ move with the specific relative drift $\mathbf{U}$, causing momentum losses to the fluctuation field which just cancel the momentum gain in field $\mathbf{E}_0$. For a description of this situation, one can formally introduce an 'effective collision frequency', ν_{eff} (see the review by Papadopoulos, 1977) by which momentum losses and gains can be equated in the following manner:

$$e\mathbf{E}_0 = (m\mathbf{U})\nu_{\text{eff}}, \tag{3.40}$$

where $\mathbf{U}$ is the relative drift of the electrons with respect to the ions.

For the planar boundary layer treated by Fahr and Neutsch (1982a, b), this then leads to the following quantitative consequences. As is shown in Section 3.1, the change in magnitude of the magnetic field $\mathbf{B} = \mathbf{B}_x$ within the boundary layer is caused by an electrical current $\mathbf{j}_y$ that is purely in the y-direction. This current is carried by a relative motion $\mathbf{U}_y$ of the electrons with respect to the ions, yielding $\mathbf{j}_y = en\mathbf{U}_y$.

Here we first aim to calculate the effective collision frequency ν_{eff} if, as is argued by Fahr and Neutsch (1982a, b) and also strongly supported by Smith (1984) and Smith *et al.* (1984), the fluctuation field $\mathbf{E}_1$ in the layer can be assumed to be due to electrostatic wave noise. Under these conditions, the momentum loss of electrons to the wave field seen in the plasma reference system can be calculated by (Kadomtsev, 1965; Tange and Ichimaru, 1974; Papadopoulos, 1977)

$$nmU_y \nu_{\text{eff}} = \omega_{pe}^2 \sum_k 4\gamma_k W_k k \int_{-\infty}^{+\infty} \frac{[(\omega_k - kU_y) - k(v_y - U_y)]}{[(\omega_k - kv_y)^2 + \gamma_k^2]^2} f_{e,y}\, \mathrm{d}v_y, \tag{3.41}$$

where the summation runs over the wave vectors $\mathbf{k} = \mathbf{k}_y$ with imaginary wave frequencies γ_k and real wave frequencies ω_k. The energy density of the fluctuation field $\mathbf{E}_{1k}$ is denoted by W_k, and $f_{e,y}$ is the one-dimensional, v_x-, v_z-integrated electron velocity distribution function for velocity components v_y. From Equation (3.41) the effective frequency ν_{eff} can be obtained in the following form:

$$\nu_{\text{eff}} = \frac{4\omega_{pe}^2}{mU_y n} \sum_k \gamma_k W_k k [\phi_1(k, U_y) + \phi_2(k, U_y)] , \tag{3.42}$$

where the two functions $\phi_1(k, U_y)$ and $\phi_2(k, U_y)$ are defined by:

$$\phi_1(k, U_y) = \frac{1 - \overline{U}_y}{\omega_k^3} \int_{-\infty}^{+\infty} \frac{f_{e,y}\, \mathrm{d}v_y}{[(1 - \bar{v}_y)^2 + \varepsilon_k^2]^2} \tag{3.43}$$

and

$$\phi_2(k, U_y) = \frac{-1}{\omega_k^3} \int_{-\infty}^{+\infty} \frac{(\bar{v}_y - \overline{U}_y) f_{e,y}\, \mathrm{d}\bar{v}_y}{[(1 - \bar{v}_y)^2 + \varepsilon_k^2]^2} . \tag{3.44}$$

In the above formulas, all velocities with a bar on top are normalized with the phase velocity $w_k = \omega_k/k$, and ε_k is given by:

$$\varepsilon_k^2 = \left(\frac{\gamma_k}{\omega_k}\right)^2 . \tag{3.45}$$

The integrals ϕ_1 and ϕ_2 may be evaluated in the system moving with the bulk of the electrons where $f_{e,y}$ may be represented by a simple Maxwellian corresponding to a temperature T_{ey} or perhaps a superposition of two Maxwellians with temperatures T_{ey} and $T_{ey}^* \gg T_{ey}$ in order to simulate core and halo electron distributions, as for instance found in the solar wind plasma (see, for example, Feldman *et al.*, 1981). Hence, for either a mono-Maxwellian distribution or for each Maxwellian component separately one obtains:

$$\phi_1(k, U_y) = \frac{(1 - \overline{U}_y)}{\overline{V}_t \omega_k^3 \sqrt{\pi}} \int_{-\infty}^{+\infty} \frac{e^{-(\chi/\bar{v}_t)^2}\, \mathrm{d}\chi}{[(1 - \chi)^2 + \varepsilon_k^2]^2} \tag{3.46}$$

and

$$\phi_2(k, U_y) = \frac{1}{\overline{V}_t \omega_k^3 \sqrt{\pi}} \int_{-\infty}^{+\infty} \frac{(\overline{U}_y - \chi) e^{-(\chi/\bar{v}_t)^2}\, \mathrm{d}\chi}{[(1 - \chi)^2 + \varepsilon_k^2]^2} . \tag{3.47}$$

Here again the bars indicate normalizations with the phase velocity w_k. The quantity

$\bar{v}_t$ is the normalized thermal velocity:

$$v_t = \frac{\sqrt{\frac{2kT_{ey}}{m_e}}}{w_k}. \tag{3.48}$$

with the core electron temperature component T_{ey}.

There exists a good justification to reduce the summation over the unstable wave vectors **k** to only one term of the sum representing the electron interaction with the most unstable wave mode $\mathbf{k}_0$ only because this is the mode that has by far the most effective energy exchange with the plasma. From the well-known two-stream instability theory, one can derive that the imaginary part of the wave frequency connected with k_0 is given by

$$\gamma_{k_0} = \omega_{pe} \frac{\sqrt{3}}{2} \sqrt[3]{\frac{m_e}{4m_i}} \tag{3.49}$$

and that the phase velocity w_{k0} of such a wave mode is connected with the relative drift velocity U_y by:

$$U_y = w_{k_0} = \frac{\omega_{k0}}{k_0} = \frac{\omega_{pe}}{k_0}. \tag{3.50}$$

In view of the necessity to take into account the situation of a core- and halo-population of electrons, their velocity distribution function may be satisfactorily represented by a multi-temperature Maxwellian with temperature components $T_{e,i}$ in the form:

$$f_{e,y}(\chi) = \frac{1}{\sqrt{\pi}} \sum_i \varepsilon_i \exp[-\chi^2 \xi_i] \tag{3.51}$$

where the quantity ξ_i is given by:

$$\xi_i = T_{e,y}/T_{e,i} \tag{3.52}$$

and where ε_i defines the relative fraction of the component with $T_{e,i}$ of the total electron content. If the summation over the wave vectors **k** in Equation (3.41) is reduced to only the most unstable wave mode with $\omega_{k0} = \omega_{pe}$ and $k_0 = \omega_{pe}/U_y$, and if the distribution function (3.51) is used, one arrives at the following expression:

$$\begin{aligned} nm_e U_y \nu_{\text{eff}} &= 4\omega_{pe}^2 \gamma_{k_0} W_{k_0} k_0 \sum_i \varepsilon_i \phi_{2,i}(k_0, \overset{*}{U}_y) \\ &= \sqrt[3]{\frac{m_e}{4m_i}} \sqrt{\frac{12}{\pi}}\, \omega_{pe} \frac{W_{k0}}{U_y} \overset{*}{U}_y \sum_i \varepsilon_i \sqrt{\xi_i} \int_{-\infty}^{+\infty} \frac{(1-\chi) e^{-\chi^2} \overset{*}{U}_y^2 \xi_i \, d\chi}{[(1-\chi)^2 + \varepsilon_k^2]^2} \\ &= \sqrt[3]{\frac{m_e}{4m_i}} \sqrt{\frac{12}{\pi}}\, \omega_{pe} \frac{W_{k0}}{U_y} \overset{*}{U}_y \sum_i \varepsilon_i J_i(\overset{*}{U}_y). \end{aligned} \tag{3.53}$$

Here $\overset{*}{U}_y$ is the ratio of the relative drift U_y and the thermal velocity defined with Equation (3.48)

$$\overset{*}{U}_y = U_y/v_t \,. \tag{3.54}$$

The value of the integral $J_i(\overset{*}{U}_y)$ can be calculated as the imaginary part of a known complex analytic function and is given by

$$J_i(\overset{*}{U}_y) = \frac{\pi \overset{*}{U}_y \sqrt{\xi_i}}{\varepsilon_{k0}} \chi_i(\chi_i e^{\chi_i^2} \operatorname{erfc}(\chi_i)) \quad \text{with} \quad \chi_i = \overset{*}{U}_y \sqrt{\xi_i}(\varepsilon_{k0} + i)\,, \tag{3.55}$$

where i is the imaginary unit.

According to the results obtained by Davidson *et al.* (1969), it may be assumed that for a saturated wave field, the fluctuation field energy density W_{k0} is connected with the relative drift U_y by:

$$W_{k0} = \tfrac{1}{2} n m_e U_y^2 \,. \tag{3.56}$$

If the momentum losses due to Equation (3.55) are balanced by gains from a static electric field E_{0y} seen in the plasma rest frame that moves with a velocity U_z perpendicular to the local magnetic field $\mathbf{B} = \mathbf{B}_x$ (see Fahr and Neutsch, 1982a, b), it follows that

$$eE_{0y}(z) = \frac{e}{c} |U_z B_x|_z = \frac{eK}{c} \left|\frac{B_x}{\rho}\right|_z =$$

$$\sqrt[3]{\frac{m_e}{4m_i}}\, \omega_{pe} \sqrt{\frac{12}{\pi}}\, \frac{m_e \overset{*}{U}_y v_t}{2} \sum_i \varepsilon_i J_i(\overset{*}{U}_y) \,. \tag{3.57}$$

This now has to be considered as an implicit equation for $\overset{*}{U}_y = \overset{*}{U}_{y0}$. It has to be solved locally, i.e., for each value z within the boundary layer where a specific value for $E_{0y}(z)$, i.e., of B_x and ρ, is attained. After the determination of the local value of $\overset{*}{U}_{y0}$ with the help of Equation (3.57), one can calculate the effective frequency by:

$$\nu_{\text{eff}} = \sqrt[3]{\frac{m_e}{4m_i}}\, \omega_{pe} \sqrt{\frac{\overset{*}{U}_{y0}}{\pi}}\, \frac{}{2} \sum_i \varepsilon_i J_i(\overset{*}{U}_{y0}) \tag{3.58}$$

and will obtain the electrical conductivity σ_{eff} by:

$$\sigma_{\text{eff}} = \frac{\omega_{pe}^2}{4\pi \nu_{\text{eff}}} = \frac{\omega_{pe}}{4} \sqrt[3]{\frac{4m_i}{m_e}}\, \frac{1}{\sqrt{3\pi}\, \overset{*}{U}_{y0} \sum_i \varepsilon_i J_i(\overset{*}{U}_{y0})} \,. \tag{3.59}$$

3.4. Derivation of Specific Solutions for the Heliopause Transition Layer

From the hybrid MHD-theory of a plasma contact discontinuity presented in Section 3.1, we have derived a set of solutions for the density ρ, the diffusion velocity U_z and the magnetic field $B = B_x$ as functions of the coordinate z (z-axis perpendicular

to the boundary layer as illustrated in Figure 2). The corresponding solutions given by Equations (3.18) through (3.21) were obtained as functions of an auxiliary independent variable ϕ. The introduction of ϕ is advisable to transform the elliptical integral in Equation (3.16) into its more suitable Legendre–Jacobi form. In Figure 7 we have displayed the quantities z, ρ, B, and E_z as functions of this variable ϕ.

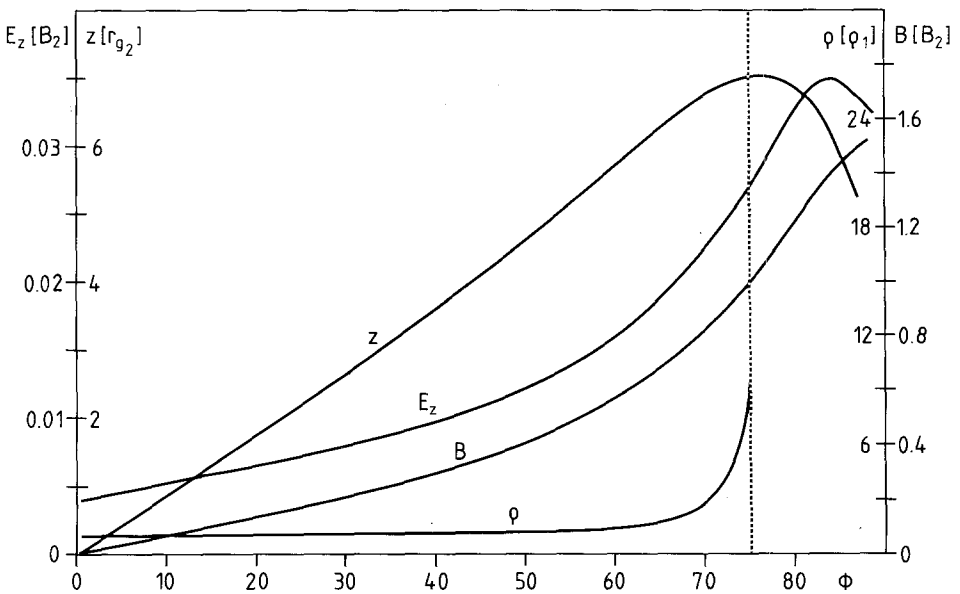

Fig. 7. A set of consistent solutions of the two-fluid plasma equations including sheath position z, electric field E_z in a normal direction (i.e., z-direction), magnetic field B in y-direction, and the plasma mass density as functions of the auxiliary variable Φ is given. The dotted vertical line indicates $\Phi = \Phi_{max}$, i.e., the outer boundary $z = Z$ of the layer. Input data are mentioned in the text.

The relation of the variable ϕ to the location z within the layer could then be obtained with Equation (3.19). This relation varies for different values of the relevant boundary layer parameters K, G, and Γ. As is evident from Equation (3.19), the coordinate z always attains a maximum value $z = Z$ for a specific value $\phi = \phi_2$ determined by:

$$\sin^2 \phi_2 = \frac{2\Gamma}{\Gamma + 1} \frac{\mu - 1}{\mu\Gamma - 1}, \tag{3.60}$$

with μ given by $\mu = \rho_2/\rho_1$. Z has the physical meaning of the total thickness of the layer. As one may recognize in view of Equation (3.60), Z is a function of the parameter Γ and the density ratio μ. In Figure 8 we have shown this dependence of the sheath dimension Z on the parameter Γ. Since this parameter unfortunately can be fixed only with some difficulty, as is evident from its definition in Equation (3.24), it may be of interest to note that the solutions plotted in Figure 7 are scaled with Z.

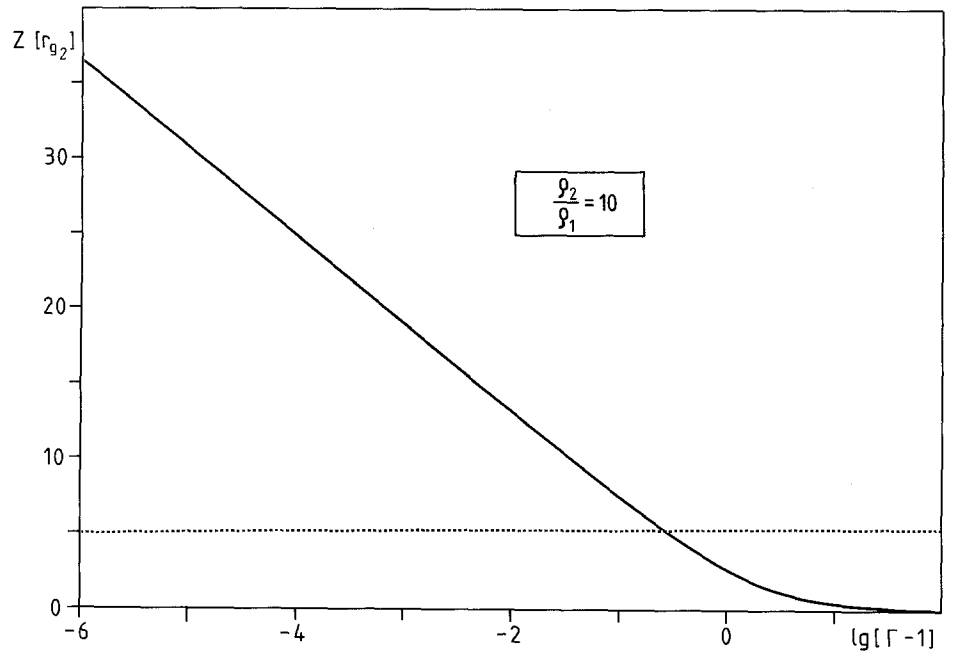

Fig. 8. The Z-dimension of the heliopause boundary layer is given, in units of gyroradii at the interstellar side, as a function of the family parameter Γ. A ratio of 10 between outer and inner densities was adopted.

For the specific transition layer parameters calculated at the end of Section 3.4, i.e.:

$$K^2 = 9.27 \times 10^{-40}[\mathrm{g\,cm^{-2}\,s^{-1}}];$$

$$G = 3.59 \times 10^{-13}[\mathrm{G \times G}], \qquad \Gamma = 1.0763,$$

Figure 9 shows the quantities ρ and B as functions of the coordinate z.

From Equation (3.8), one can also derive an expression for the z-component of the stationary electric field, i.e., E_z, which is expressed as a function of ρ and B in the following form:

$$E_z(z) = \frac{-m_i}{e\rho}\left(\frac{B^2}{8\pi}\right)' + \frac{Am_i}{e\rho}\left|\frac{k_B T_0}{m_e}\rho^2 + \frac{K^2}{2}\right|^{-1/2}. \tag{3.61}$$

Using the definition for the constant G in Equation (3.11), the electric field E_z thus can also be expressed by a pure function of ρ and its derivative with respect to the coordinate z:

$$E_z(z) = -\frac{3}{2}\frac{m_i}{e}\frac{K^2}{\rho^3}\rho' + \frac{Am_i}{e\rho}\left|\frac{k_B T_0}{m_e}\rho^2 + \frac{K^2}{2}\right|^{-1/2}. \tag{3.62}$$

The quantity A in Equations (3.61) and (3.62) is given by the following explicit

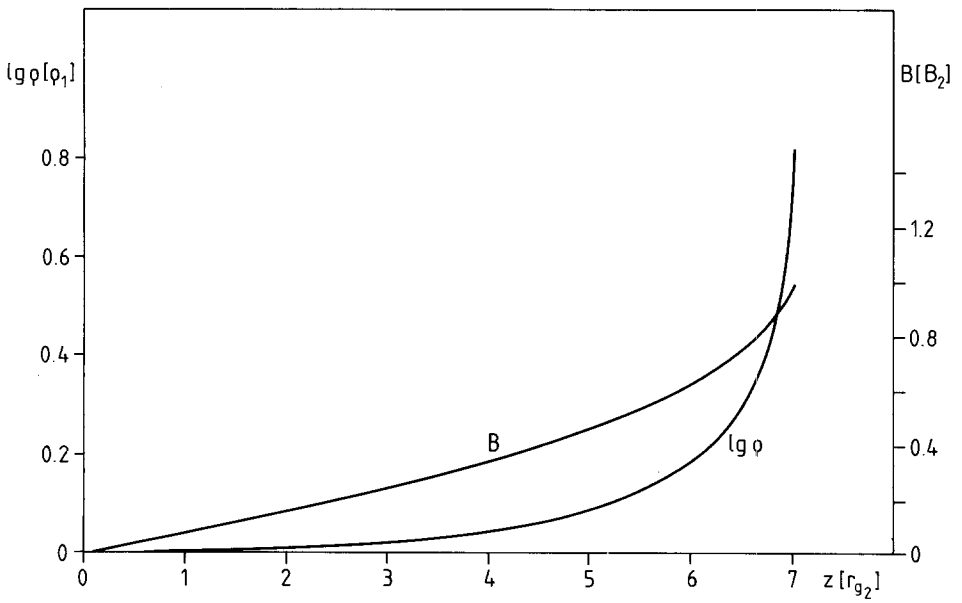

Fig. 9. The density and the magnetic field are shown as functions of position z in the boundary layer. See text for input quantities that were adopted here.

expression:

$$A = J(0)\gamma_{k0}\left(\frac{m_e}{m_i}\right)K^2 = \omega_{pe}\,\frac{\sqrt{3}}{2}\,\sqrt[3]{\frac{m_e}{4m_i}}\left(\frac{m_e}{m_i}\right)K^2\,, \tag{3.63}$$

where $J(0) = J(\overset{*}{U}_y = 0) = 39.905$ and is identical with the integral $J(\overset{*}{U}_y)$ defined in Equation (3.52) for $\overset{*}{U}_y = 0$.

In Figure 10, the electric field component E_z normalized with B_z is shown as a function of z for the above-quoted transition layer parameters. As is evident, the electric field E_z everywhere in the layer represents less than 3% of the magnetic field B_2 at the interstellar side. Nevertheless, in view of the fact that the field on the solar side has been calculated with a value of $B_1 = 8 \times 10^{-7}$ G (about a factor of 4 smaller than at the interstellar side), this means that the electric field $E_z = E_{z1}$ at the solar side may not be considered as totally negligible with respect to B_1.

With the demand that the electric field E_z vanishes at the solar side, one could use Equation (3.61) as a definition for the magnetic field gradient value $|\mathrm{d}B/\mathrm{d}z|_{z_1} = B_1'$. This yields the formula:

$$B_1' = \frac{1}{B_1}\,\frac{4\pi J(0)\gamma_{k0}\left(\frac{m_e}{m_i}\right)K^2}{\sqrt{\frac{k_B T_0}{m_e}\,\rho_1^2 + \frac{K^2}{2}}}\,. \tag{3.64}$$

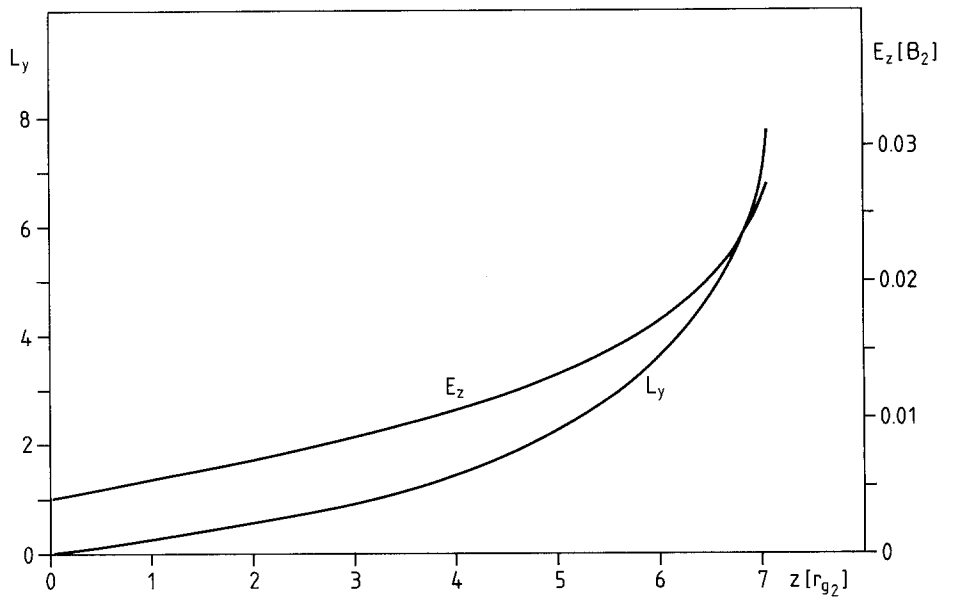

Fig. 10. The electric field in z-direction and the electric energy L_y dissipated per unit of time and space are shown as functions of position z in the boundary layer.

With this formula and the boundary values adopted in Section 3.1, we would arrive at $B_1' = 3.85 \times 10^{-12}[\mathrm{G/cm}^{-1}]$, which in comparison to the value calculated in Section 3.1 appears fairly large. However, it is small enough that it does not change the results concerning Γ calculated by Equation (3.24) and thus does not change anything in the set of solutions presented.

In connection with the electric current j_y needed to reduce the magnetic field $\mathbf{B} = (B_x, 0, 0)$, an electric energy $L_y(z)$ is dissipated per unit time and unit volume due to Ohmic heating in the layer. This quantity $L_y(z)$ can be calculated with the help of the expression:

$$L_y(z) = j_y(z)E_y(z)\,. \tag{3.65}$$

Here the current j_y is given by the corresponding Maxwell equation, and E_y is the stationary electric field in the y-direction that has to compensate for the Lorentz forces acting upon the plasma that moves with the velocity U_z perpendicular to the magnetic field B_x. Thus, one obtains the dissipated energy in the form:

$$L_y(z) = \left(\frac{c}{4\pi}\frac{\mathrm{d}B}{\mathrm{d}Z}\right)\left(\frac{1}{c}\,U_z B\right) = \frac{1}{4\pi}\,\frac{K}{\rho}\,B\,\frac{\mathrm{d}B}{\mathrm{d}z}\,, \tag{3.66}$$

which, with the use of Equations (3.18) through (3.21), can be calculated explicitly by:

$$L_y(z) = \frac{\Gamma^2 - 1}{\Gamma}\sqrt{\frac{2gG}{3\Gamma}}\,\frac{\sin\phi\cos\phi(1 - \Gamma k^2\sin^2\phi)}{k^2(1 + \cos^2\phi) - 1}\,(1 - k^2\sin^2\phi)^{-3/2}\,. \tag{3.67}$$

This quantity is shown in Figure 10 as a function of the coordinate z. It indicates that the main energy dissipation takes place at the interstellar side of the layer where both the magnetic field magnitude and its gradient with z attain maximum values.

As was also mentioned in Section 3.3, one can derive the relative drift velocity U_y in y-direction between electrons and ions as a function of the position z in the layer from the implicit Equation (3.55). For calculation prurposes, we have to fix some constants that describe the distribution function $f_{e,y}$ of the electrons in the layer. As was discussed in the previous section, we have approximated $f_{e,y}$ as a multi-Maxwellian according to an expression given in Equation (3.51). With this expression we aimed at an as realistic representation as possible of the core-halo-electron population following from observational results of Feldman (1981) and Pilipp (1983). In view of the results by Feldman (1981), we shall favour the following form for $f_{e,y}$:

$$f_{e,y}(\chi) = \frac{1}{\sqrt{\pi}} \sum_{i=1}^{2} \varepsilon_i e^{-\chi^2 \xi_i}, \tag{3.68}$$

with

$$\varepsilon_1 = 0.96; \quad \xi_1 = 65.0; \quad T_{e,y} = 10^4 \text{ K};$$
$$\varepsilon_2 = 0.04; \quad \xi_2 = 0.85 .$$

With this representation for $f_{e,y}$, Equation (3.55) can be evaluated to determine the consistent relative drift U_y as a function of z using the results already obtained for ρ and B in Figure 9. In Figure 11, the result for this thermally normalized drift, $\overset{*}{U}_y$, is shown

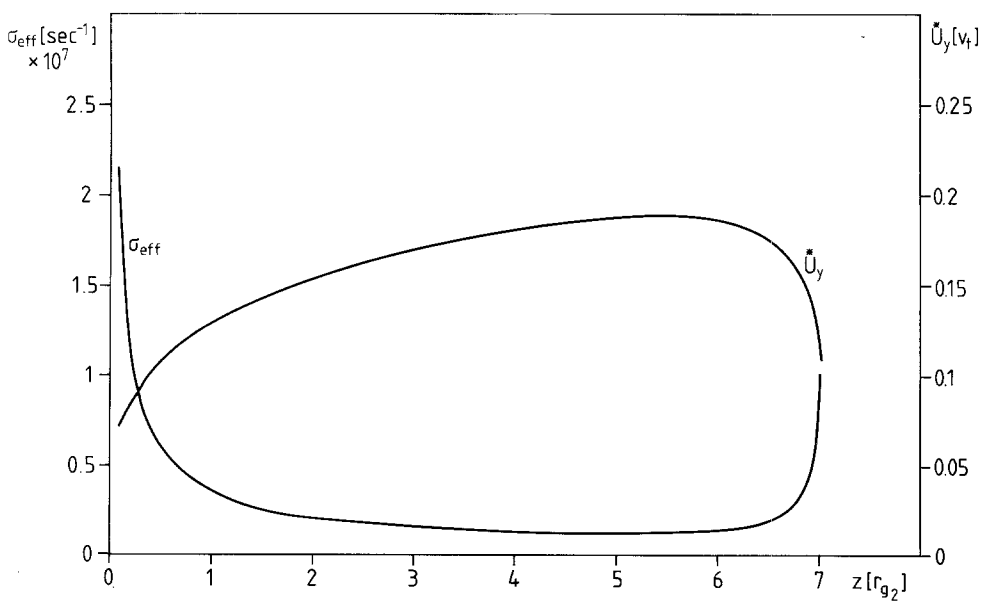

Fig. 11. The relative drift velocity U_y of electrons is shown with respect to protons in y-direction, normalized with the thermal velocity of the electrons, and the effective electrical conductivity σ_{eff} as functions of the position z in the boundary layer, measured in units of 10^7 s^{-1}.

versus z. Here it is interesting to mention that changes in ε_2 and ξ_2 in the framework of experimentally discussed uncertainties cause only a very minor change in $\overset{*}{U}_y$ in the range of less than 1%.

In connection with these results for $\overset{*}{U}_y$, one can use Equation (3.57) to derive a result for the effective electric conductivity $\sigma_{\text{eff}}(z)$. These results are plotted in Figure 11 from which it may be seen that σ_{eff} varies surprisingly little over the whole extent of the layer and attains a very low value near an average of only $\langle \sigma_{\text{eff}} \rangle = 2 \times 10^6\ \text{s}^{-1}$. Only at the innermost and outermost regions does σ_{eff} increase sharply to values of $> 2 \times 10^7\ \text{s}^{-1}$. As a representative value for the layer, one may, however, adopt a value of $\langle \sigma_{\text{eff}} \rangle = 2 \times 10^6\ \text{s}^{-1}$, which in comparison to corresponding classic conductivity values defined by Spitzer (1956) or Braginski (1957) is six orders of magnitude lower.

With this low conductivity, caused by the effective electrostatic plasma-wave coupling, one would arrive with the help of Equation (3.36) at the following value α for the magnetic reconnection probability coefficient:

$$\alpha = \frac{4}{R_m} \frac{V_{a2}^2}{V_{A2}^2 + \frac{3}{2}C_{s2}^2} = \frac{c^2}{ZV_{A2}\sigma_{\text{eff}}} \frac{V_{a2}^2}{V_{A2}^2 + \frac{3}{2}C_{S2}^2} = 9.5 \times 10^{-2}. \tag{3.69}$$

4. Transport of Plasma Due to Reconnection Processes

4.1. Evaluation of the Average Rate of Transport: Analogy to the Magnetopause

An alternative way of estimating the efficiency of plasma transport through the heliopause is to look for analogous situations in space where a discontinuity surface (layer with strong gradients) separates two plasmas of disparate origin and physical state. As was recently suggested by Macek and Grzedzielski (1985), the situation at the heliopause may very much resemble that prevailing at the downwind side of planetary magnetospheres with developed long magnetospheric tails. There we also have two different plasmas, dense solar wind and rarefied lobe plasma, interacting in the first approximation only via pressure forces, i.e., by equalizing the normal component of the total pressure (condition for tangential discontinuity). As was amply demonstrated in decades of space experiments, the boundary eventually becomes 'leaky' and both plasma and magnetic flux are transported across it (for a review of plasma mixing at the terrestrial magnetopause, cf. Cowley, 1982).

To stress the perceived similarities between the boundaries of the distant terrestrial and Jovian tails and the heliopause, we show in Table II the characteristic data of the plasma regimes in question. In rows I and II, the characteristic plasma values for the distant terrestrial magnetotail and the distant Jovian tail, respectively, are indicated. Row III corresponds to the expected heliopause conditions. The values for Earth are based on data obtained from the recent ISEE-3 passes through the deep magnetotail at 60–240 Earth radii from the planet.

Typical plasma parameters measured by the ISEE-3 in the deep geomagnetic tail at

TABLE II

The change of the typical plasma-field conditions from the outer solar (interstellar) wind to the inner magnetospheric (heliospheric) side of the interfaces for the cases of: I. Terrestrial magnetosphere; II. Jovian magnetosphere; and III. Solar heliosphere

Interface at		Density (cm^{-3})		Temperature (eV)		Magnetic field (G)		Tangential velocity difference ($km\ s^{-1}$)
		n_1 (inner)	n_2 (outer)	k_BT_1 (inner)	k_BT_2 (outer)	B_1 (inner)	B_2 (outer)	
I	Earth (tail)	4×10^{-2}[a]	7	$\sim 10^2$[a]	~ 10	9×10^{-5}[a]	6×10^{-5}	200–300
II	Jupiter (tail)	3×10^{-3}[b]	$(1–2) \times 10^{-1}$	$\sim 2 \times 10^2$[b] $\sim 6 \times 10^2$	~ 2	$(1–2) \times 10^{-6}$[b]	5×10^{-6}	100–200
III	Front heliosphere	10^{-3}	10^{-1}	$\sim 2 \times 10^2$	~ 2	$\sim 10^{-6}$	$(1–3) \times 10^{-6}$	100–200

[a] Lobe values.
[b] Core values.

$\sim 200R_e$ (lobe) are: density $n_1 \simeq 0.04\,\mathrm{cm}^{-3}$, the electron temperature $\sim 8 \times 10^5$ K (Bame *et al.*, 1983) and the average tailward component of the tail lobe field is fitted to $B_1 = 9.1 \times 10^{-5}$ G (Slavin *et al.*, 1983). The average solar wind (outer) ion and electron temperatures: are $T_i = 8 \times 10^4$ K, $T_e = 1.5 \times 10^5$ K (Slavin *et al.*, 1983).

The plasma parameters measured by Voyager 2 in the distant Jovian magnetotail at 3–4 AU behind Jupiter (core) are typically: density $n_1 \sim 3 \times 10^{-3}\,\mathrm{cm}^{-3}$ and magnetic field $B_1 = (0.1\text{–}0.2) \times 10^{-5}$ G (Kurth *et al.*, 1982). The average solar wind (outer) magnetic field during the Voyager 2 mission was $B_2 = 4.5 \times 10^{-5}/r$ G where the heliocentric distance r is given in AU (Burlaga *et al.*, 1982), and plasma density $n_2 \sim (1\text{–}2) \times 10^{-1}\,\mathrm{cm}^{-3}$ (at ~ 3 AU, Lepping *et al.*, 1982). The average tail temperature was estimated in two ways: from the pressure balance with the standard solar wind, one obtains $kT_1 \sim 0.2$ keV, and from the solar wind kinetic energy dissipation corresponding to the velocity jump across the distant Jovian magnetopause (from 450 to 300 km s^{-1}, Lepping *et al.*, 1982; Figures 4 and 10) follows $kT_1 \sim 0.6$ keV.

Table II shows that the rarified heliospheric plasma (side 1) corresponds to the tail cavity plasma, while the LISM wind (side 2) can be regarded as the equivalent of the magnetosheath plasma flow. In close and logy to the case of the magnetospheric boundary treated by Grzedzielski and Macek (1984), the most straightforward method of inferring the corresponding efficiency of plasma transport across a semi-permeable boundary is to estimate the *average* rate of gradual filling-up of the magnetospheric cavity by the external LISM plasma as one proceeds from the planet down into the distant magnetospheric tail. To relate the observed tail plasma and magnetic field values to the transport properties at the boundary, one can make use of a time-independent model of the cavity and assume that the observed cavity plasma densities correspond to an equilibrium situation when all sources of plasma are balanced by the sink which is believed to be due to plasma expansion along the tail. Using as a basis the model of Grzedzielski and Macek (1984), for the magnetotail, the tail (or rather each of its lobes) can be shown to be a long wind-hoselike structure whose cross dimensions are small compared with its length measured from the planet by the x-coordinate (Figure 12). The tail cross section at x is $A(x)$ and the total surface area of the tail's boundary from the 'nose' to x is $S(x)$.

In analogy to the magnetospheric case, the heliospheric plasma in the tail at x comes from the Sun itself or/and from the LISM plasma. The tailward mass flux of this plasma at x (beyond the neutral line in the plasma sheet) is

$$F(x) = \int_{A(x)} (\rho \mathbf{U} \mathbf{n}^{(A)})\, \mathrm{d}\Sigma^{(A)} = F_0 + \int_{S(x)} \rho^{(S)} (\mathbf{U}^{(S)} \cdot \mathbf{n}^{(S)})\, \mathrm{d}\Sigma^{(S)}\,, \tag{4.1}$$

where F_0 is the plasma loss from the planet and the second term is the total flow of plasma across the boundary $S(x)$. This second term would have vanished were $S(x)$ a tangential discontinuity in the strict sense of the word. $\mathbf{n}^{(S)}$, $\mathbf{n}^{(A)}$ denotes here the (outward pointing) unit vector normal to the surface elements $\mathrm{d}\Sigma^{(S)}$, $\mathrm{d}\Sigma^{(A)}$ of the surfaces S and A. ρ and $\mathbf{U}$ without superscripts refer to the tail values, those with

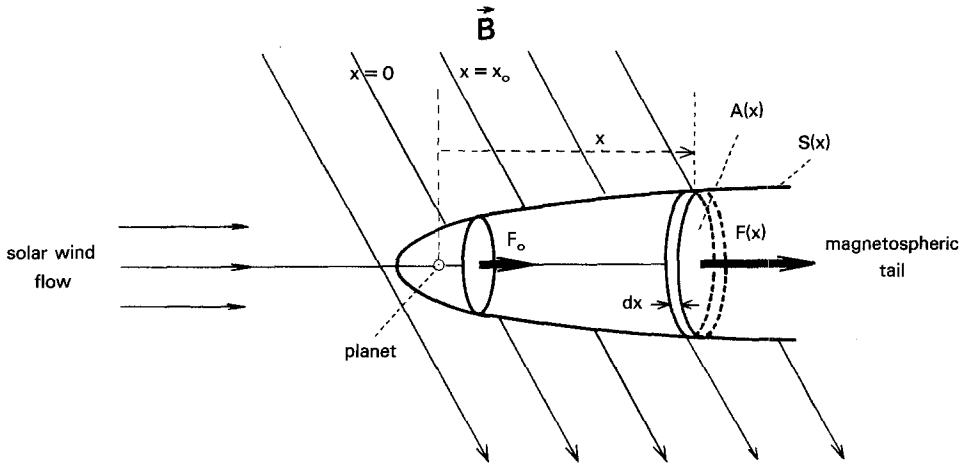

Fig. 12. Illustrative view of the tail magnetopause imbedded in the solar wind plasma flow. All quantities that are used in the text are indicated.

superscripts S, A to the values at surfaces S, A. It then follows that the effective speed of diffusion of plasma through the boundary (cf. Section 1.2.2) can be written as $U_D = |\mathbf{U}^{(S)} \cdot \mathbf{n}^{(S)}|$.

In this section we, furthermore, assume that the dominant mechanism of plasma diffusion across the magnetospheric boundary is turbulence resulting from the reconnection of magnetic lines of force, as is at present recognized for the magnetosphere on the basis of experimental data (Paschmann *et al.*, 1979; Russell and Elphic, 1979; Sonnerup *et al.*, 1981; Cowley, 1982). We should also like to call attention to the high values for the diffusion speed U_D obtained in the reconnection-related tearing mode instability turbulence in the available theoretical estimates (cf. Section 1.2.2, Equations (1.12) and (1.13)). There is also evidence that reconnection does not occur uniformly but in 'patches' or 'windows' (Russell and Elphic, 1979; Winterhalter *et al.*, 1981), and its occurrence is strongly dependent on the relative orientation of the external and internal magnetic field vectors (Berchem and Russell, 1984).

Returning now to the analogous case of the magnetopause (Grzedzielski and Macek, 1984), the current attempts to model theoretically the flow of plasma through a reconnection area are based on the assumption that the magnetopause boundary in these regions is a rotational discontinuity rather than a tangential one (Sonnerup and Ledley, 1974; Lee and Roederer, 1982; Scudder, 1984; Heyn *et al.*, 1985). In the most simple case of a rotational discontinuity, i.e., in an isotropic and locally homogeneous plasma, one has

$$(\mathbf{U}^{(S)} \cdot \mathbf{n}^{(S)}) = (\mathbf{B}^{(S)} \cdot \mathbf{n}^{(S)})/(4\pi\rho^{(S)})^{1/2}, \tag{4.2}$$

where $\mathbf{B}^{(S)}$ is the magnetic field on S and $|\mathbf{B}^{(S)} \cdot \mathbf{n}^{(S)}| = B_n^{(S)}$ is the normal (interconnecting) component of the magnetic field in the boundary layer.

Let us now define α to be the fraction of the external (draped) solar wind magnetic field, averaged over the lateral area $dS(x)$ of the slice Adx (hatched in Figure 12) that

becomes connected to the internal tail field by diffusion across the boundary. For a rotational discontinuity, α can be identified, in view of Equation (4.2), with the reconnection parameter introduced in Section 3 (Equation (3.38)). If one further approximates the magnitude of the draped solar wind field by the average azimuthal component B_φ of the interplanetary spiral magnetic field and puts $\rho^{(S)} \simeq \rho_{SW}$ (Grzedzielski and Macek, 1984), one has $B_n^{(S)} = \alpha B_\varphi$ and from Equation (4.2)

$$\alpha = \frac{U_D}{B_\varphi/(4\pi\rho_{SW})^{1/2}} = \frac{U_D}{V_{A_\varphi}}, \tag{4.3}$$

where indices SW stand for solar wind. V_{A_φ} denotes here the solar wind Alfvénic speed associated with the azimuthal component of the interplanetary field (typically one has $V_{A_\varphi} = V_{ASW}$ (solar wind) $\simeq 25$ km s^{-1}).

Introducing the relationship (4.3) into Equation (4.1), one has

$$\int_{A(x)} \rho(\mathbf{U}\mathbf{n}^{(A)})\, d\Sigma^{(A)} = F_0 + \langle\alpha\rangle \int_{S(x)} \rho_{SW} V_{A_\varphi}\, d\Sigma^{(S)}, \tag{4.4}$$

where

$$\langle\alpha\rangle = \frac{\int_{S(x)} \rho_{SW}\alpha V_{A_\varphi}\, d\Sigma^{(S)}}{\int_{S(x)} \rho_{SW} V_{A_\varphi}\, d\Sigma^{(S)}}, \tag{4.5}$$

is the average value of α over $S(x)$. If one further denotes by ρ_{av} the average (mass) plasma density in the slice

$$\rho_{av} \equiv \frac{\int_{A(x)} \rho\mathbf{U}\mathbf{n}^{(A)}\, d\Sigma^{(A)}}{\int_{A(x)} \mathbf{U}\mathbf{n}^{(A)}\, d\Sigma^{(A)}}, \tag{4.6}$$

one immediately obtains from Equation (4.4)

$$\langle\alpha\rangle = \frac{\rho_{av} \int_{A(x)} \mathbf{U}\mathbf{n}^{(A)}\, d\Sigma^{(A)} - F_0}{\int_{S(x)} \rho_{SW} V_{A_\varphi}\, d\Sigma^{(S)}}. \tag{4.7}$$

To make use of this relationship between $\langle\alpha\rangle$ and ρ_{av}, one has to know $A(x)$, $S(x)$, and $U(x)$. These can be found assuming that the shape of the tail boundary is on the

whole determined by the condition of equality of the normal components of the hydromagnetic stress tensors on both sides of the boundary (pressure equilibrium) and $U(x) \sim V_{SW}$ (Grzedzielski *et al.*, 1986). Effective shapes were found, both for circular and noncircular tail cross sections, that reasonably predicted the dimensions inferred later from the observations of the Jovian tail (Grzedzielski *et al.*, 1981, 1982; Macek and Grzedzielski, 1984) and that agree with those measured for the distant terrestrial tail (Grzedzielski *et al.*, 1986). Now assuming that ρ_{av} can be identified with the *observed* average plasma density in the distant tail (2–3) $\times 10^{-2}$ cm^{-3} in the case of Jupiter (Voyager data) and $\lesssim 1$ cm^{-3} in the case of Earth (ISEE-3 data), one obtains for both objects (Grzedzielski and Macek, 1984; Macek and Grzedzielski, 1985), essentially the same value of

$$\langle \alpha \rangle \simeq 10^{-1}. \tag{4.8}$$

The same reasoning can be applied to the loss of magnetic flux from the tail. Although it may be questionable whether this kind of difference is significant in view of all the uncertainties involved, we should like to note that it may indicate that the plasma inflow velocity and the normal component of the magnetic field are not related by the simple expression (4.2), i.e., that the anisotropy of plasma changes across the boundary.

The average value of the reconnection parameter $\langle \alpha \rangle \sim 10^{-1}$ obtained from the balance of plasma sources and sinks in the magnetospheric cavities is in reasonable agreement with the theoretical estimates resulting from Galeev's tearing mode instability turbulence (cf. Sections 1.2.2, Equations (1.12) and (1.13)), especially if one recalls that the reconnection patches definitely will cover only a fraction of the total area. Similarly, this rate of reconnection can well accommodate the Sonnerup (1970) dynamical fluid type solution that allows α to be locally as high as $1 + \sqrt{2}$. It is also interesting to note that the value $\alpha \sim 10^{-1}$ can be obtained quite independently on the basis of a solution for the heliopause structure that invokes electrostatic turbulence as the most relevant process, as was discussed in Section 3; this sheds some light on the underlying physics. We, therefore, feel that there are strong reasons for the expectation that the speed (averaged over a large area) with which the external plasma may cross the heliopause may be smaller than the Alfvén velocity, but probably by no more than one order of magnitude.

4.2. Specific reconnection pattern at the heliopause

If reconnection of the magnetic fields is the source of plasma diffusion across the heliopause, one can expect effects related to the geometry of the fields on both sides. This question recently became a topic of study in magnetospheric physics (Crooker, 1979; Luhmann *et al.*, 1984a, b) as a result of the available evidence for a non-uniform distribution of reconnection patches and their dependence on the sign of the z-component of the interplanetary magnetic field (Cowley, 1982; Berchem and Russell, 1984).

In this section we give a simple qualitative picture of the expected reconnection patterns on the frontal heliopause assuming that the reconnection areas depend on the angle Ψ between the magnetic field vectors draped on the inner (side 1) and outer

(side 2) surface of the heliopause layer. The reconnection patch is defined by the condition

$$\Psi > \frac{\pi}{2}. \tag{4.9}$$

The model is based on the following assumptions:

(i) The frontal heliopause is a half-sphere of radius $r = R$.

(ii) The current sheet lies in the ecliptic plane (x, y plane). This seems to be acceptable

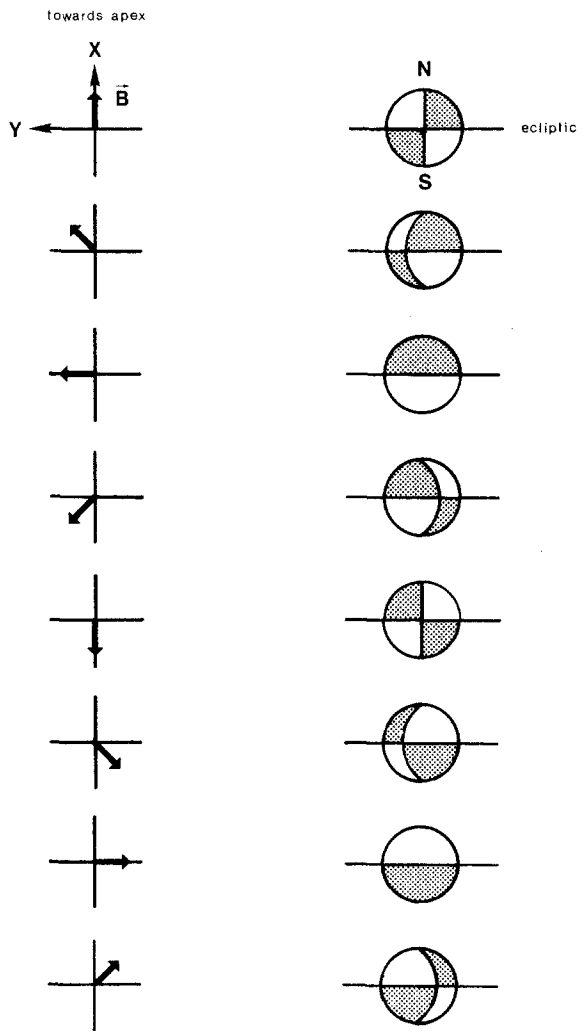

Fig. 13. A view of the heliopause front side is shown projected onto the $z - y$-plane (x-direction is collinear with the LISM wind flow vector). Depending on the orientation of the interstellar magnetic field vector $\mathbf{B}_2$, different areas, indicated by dotted areas, are expected where magnetic field reconnection takes place. The observed is thought to be located in the Sun. Ecliptic corresponds to the x-y-plane.

except for epochs of solar magnetic field reversals 2–3 yr after the solar cycle maximum (Tritakis, 1984).

(iii) The solar wind magnetic field lines (before draping) are spirals wound up on conical surfaces with the focus in the Sun. They are described by (Coleman, 1976)

$$B_r = B_0(r_0/r)^2, \qquad B_\vartheta = 0, \qquad B_\varphi = -B_0 \frac{\Omega r_0}{U_r} \frac{r_0}{r} \sin\vartheta\,, \tag{4.10}$$

φ and ϑ here are the ecliptic longitude (counted from the x-axis in the direction of solar rotation) and the ecliptic co-latitude, respectively. U_r is the constant radial velocity of the solar wind, Ω denotes the Sun's angular velocity. The radial field B_0 at a reference distance r_0 changes sign across the current sheet and, in a given hemisphere, may be either positive or negative.

(iv) The external plasma that brings the LISM magnetic field to the heliopause flows along the $(-x)$-axis ($+x$ direction corresponds to the direction from the Sun towards the apex). The plasma apex is supposed to be identical with the LISM neutral gas apex that is known to be located in the vicinity of the ecliptic plane (Bertaux, 1984).

(v) The interstellar magnetic field at large distances (before any draping, including the deflection in the sub-Alfvénic case, is uniform:

$$\mathbf{B}^{is} = (B_x^{is}, B_y^{is}, B_z^{is}) = \text{const.} \tag{4.11}$$

(vi) The draping consists of a simple projection of the field lines onto the heliopause with no distortions due to the 'heliosheath' flow or shocked solar wind flow taken into account. Note that it is only the *direction* of the draped field and not its magnitude that is required by criterion (4.9). The direction of the projected line of force, at the point of intersection of a given original line of force (Equations (4.10) or Equation (4.11)) with the sphere $x^2 + y^2 + z^2 = R^2$, is determined by the vector $\mathbf{H}$ defined by

$$\mathbf{H}_{1,2} = \mathbf{n} \times (\mathbf{B}_{1,2} \times \mathbf{n})\,, \tag{4.12}$$

where $\mathbf{n} = \mathbf{R}/R$. The projected interstellar line of force is, therefore, always contained in the plane defined by the original direction of the line and the Sun. Similarly, the projected solar wind field line always stays on its original cone. In order to express the criterion (4.12) in terms of the coordinates of the initial magnetic fields, we first find the vectors

$$\mathbf{H}_1 = B_0 \left(\frac{r_0}{R}\right)^2 \left(\frac{\Omega R}{U_r}\right) \frac{1}{R}\,(y, -x, 0)\,, \tag{4.13}$$

$$\mathbf{H}_2 = \frac{1}{R^2}\,[(y^2 + z^2)B_x^{is} - xyB_y^{is} - xzB_z^{is},$$

$$(x^2 + z^2)B_y^{is} - zyB_z^{is} - xyB_x^{is},$$

$$(x^2 + y^2)B_z^{is} - zxB_x^{is} - yzB_y^{is}]\,. \tag{4.14}$$

and

$$\mathbf{H}_1\mathbf{H}_2 = -B_\varphi(r = R)(B_z^{is} \sin\varphi - B_y^{is} \cos\varphi) . \tag{4.15}$$

Then, as condition (4.9) is equivalent to $\mathbf{H}_1\mathbf{H}_2 < 0$, the criterion for reconnection becomes

$$B_0(B_x^{is} \sin\varphi - B_y^{is} \cos\varphi) < 0 . \tag{4.16}$$

Note that in this model, B_z^{is} does not enter into the criterion for reconnection. The model, therefore, cannot be valid for the 'polar caps' of the heliosphere for which the procedure of algebraically adding B_z^{is} to the unchanged solar wind magnetic field (Akasofu and Covey, 1981) may be more appropriate.

In order to illustrate the dependence of the reconnection patches as predicted by the present model on the direction of the interstellar magnetic field for an observer in the inner heliosphere, a series of views of the frontal heliopause is given for eight directions of the external field. Each view corresponds to the outward polarity, $B_0 > 0$, in the northern ecliptic hemisphere (Figure 13). It is evident that the patches (hatched areas) strongly depend on the direction of the external field. To that picture one should add a strong reconnection patch in that polar cap whose polarity is opposite to the external field. One should also bear in mind that in a realistic situation the 'nose' of the heliopause itself may be significantly deviated from the gas flow apex if the inclined external magnetic field has an energy density comparable to the LISM plasma flow energy density (cf. Fahr *et al.*, 1985).

5. Evaluation of the Theoretical Approaches

5.1. Dependence on Time and Location

The general conclusion suggested by the discussion in Sections 2, 3, and 4 is that there seem to exist several good reasons for the expectation that the heliopause is a fairly leaky surface. Consequently, when constructing solutions for the plasma flow on both sides of the heliopause, one would have to take into account the effects of mass-, momentum-, energy-, and field flow across this surface boundary. One may also expect energy conversions from the bulk, fluid-type flow and the magnetic field into plasma turbulence, thereby creating features in the velocity distribution function that may not be unlike those encountered in the vicinity of the terrestrial magnetopause, as, for instance, the occurrence of high-velocity jets.

However, one has to be aware of the fact that some of the physical mechanisms discussed in the previous sections are to some extent mutually exclusive, since for their operation different sets of physical conditions have to be fulfilled. The question thus arises concerning the main factors that locally determine the plasma behaviour. In other words, one may ask how the picture of the heliopause may change in respect to the variations of the physical state of the plasma. These changes are due, for instance, to

temporal and spatial variations present in the distant solar wind and to varying conditions from the nose to the flanks of the heliopause.

The emergence of electrostatic turbulence in the boundary layer plasma based on two-stream type instabilities (Section 3) requires well-separated peaks in the combined ion velocity distribution function appearing in the region where the plasmas from both sides mix. However, this requirement can be relaxed if $T_e/T_i \gg 1$, as is shown by Davidson (1984). For instance, for a ratio $T_e/T_i \approx 10^2$ it would be sufficient to have a separation of the peaks in velocity space of the order of $10^{-2}\, v_{T,e}$. Although these conditions evidently may not be satisfied for all earlier heliopause models, we should nevertheless like to emphasize that in any case instances can be envisaged when a sufficient velocity spread in the ion peaks indeed occurs.

Such cases may, for instance, correspond to the situation when the solar wind dynamical pressure rises fairly suddenly after the minimum of the solar activity cycle. If a series of new pressure waves or shocks generated by the new activity cycle overlaps, the resulting pressure hump may 'crash' through the 'old' terminating shock of the solar wind and push it forward to the heliopause and beyond, carrying a solar wind type, collimated distribution of particles in the midst of LISM plasma. Suppose, for example, that there is a sudden 50% increase of the solar wind dynamical pressure. The new 'equilibrium' solution for the termination shock would correspond to an approximately 20% increase in the distance, i.e., to a shift by 40 AU if the 'old' position of the shock was at $r = 200$ AU. This may be sufficient to bring solar wind plasma into direct contact with the LISM plasma. In this context, it is appropriate to note that both the concepts of 'filtering' as well as of 'entrainment' of pressure fluctuations in the distant solar wind imply that the pressure fluctuation scales should be biased in favour of longer wavelengths at large heliocentric distances (Burlaga, 1984), thus enhancing the probability of 'survival' of separate velocity peaks.

Another case where a treatment like in Section 3 may apply is the polar heliopause. There, in epochs when the solar dipole field is aligned with the solar spin axis, the magnetic field vectors at the terminating shock are almost parallel to the flow lines, and the solar wind plasma, after having passed the shock, may still maintain a pronounced supersonic velocity peak in the direction of the magnetic field. It is also worth noting that in this configuration, the heliospheric terminal shock can be quite noisy itself, giving rise to 'upstream' waves and high-energy particles that might be interesting to look at with spacecraft going over the solar poles (like, for example, the Ulysses mission).

As for the fluid-type, Rayleigh–Taylor and Kelvin–Helmholtz instabilities discussed in Section 2, their appearance will of course also be facilitated when a sudden rise of solar wind pressure affects a large area of the heliopause. However, for these instabilities, the strength of the effective magnetic field will be paramount. From the instability criterion (Equation (2.1) in Section 2), one can immediately see that magnetic fields stronger than 10^{-6} G will suppress the Rayleigh–Taylor instability at the 'nose' for $\varepsilon = 0.1$ (Section 2) and for wave vectors $\mathbf{k} \parallel \mathbf{B}$. However, if the mutual orientation of the topologically unrelated fields $\mathbf{B}_1$ and $\mathbf{B}_2$ on both sides of the heliopause is such that it allows for a wave vector $\mathbf{k}$ perpendicular to *both* $\mathbf{B}_1$ and $\mathbf{B}_2$, then the instability is no

longer prevented by the magnetic fields. This indicates that the fluid-type instabilities may operate differently at different times, depending on the varying orientations of the solar wind field (the interstellar magnetic field assumed to be constant on time-scales of the order of the solar cycle time-scale). Only patches of such instability areas should in general occur over the frontal side of the heliopause.

The same conclusion most probably applies to the reconnection patches, as was already discussed in Section 4. The dominant factor should be the polarity of the solar field. A change of polarity would interchange blank and hatched areas in Figure 13. As was already mentioned, a strong reconnection region should be present around that heliospheric pole which is of opposite polarity to the interstellar magnetic field, unless the interstellar magnetic field is parallel to the ecliptic plane. This change in reconnection pattern, which depends on the solar magnetic polarity cycle, may provide some clues as to the direction of the interstellar magnetic field. If particle signatures related to reconnection could be detected in the very distant solar wind, they might tell something about the possible location of such patches. Another indication could be provided by the 'anomalous' component of cosmic rays that is thought to be energized by the turbulence at the heliosphere boundary. Nonradial gradients of this component, if observable, could be related to the direction of the external magnetic field.

Finally, we should like to point out that other mechanisms not mentioned in this discussion could also be of importance. One of these is the so-called gradient drift entry recently investigated in connection with the AMPTE magnetospheric experiment (Olson and Pfitzer, 1984). This kind of entry mechanism could well operate in such areas which are otherwise little affected by the mechanisms invoking fluid-type or kinetic-type instabilities. As was shown in numerical experiments carried out for the terrestrial magnetosphere (quoted authors), the entrance cone in the pitch angle space for this kind of mechanisms can be quite large (~ 1 radian), and the number of particles that enter may be significant. A numerical estimate for the heliopause, however, would be purely speculative at the present.

5.2. Influence on the Flow Line in the Vicinity of the Heliopause

The influence of a diffusion flow on the geometry of the resulting streamlines and on their relative orientation with respect to the heliopause can be studied by the equation of mass flow continuity formulated for the streamtube flow, as was done by Fahr and Neutsch (1982a, b). Following their formulation for the mass flow continuity along a stream tube defined by two neighbouring streamlines, we now arrive at the expression given below if a diffusive velocity component **U** perpendicular to the mean stream velocity **v** is to be considered (see Figure 5):

$$\frac{\partial \rho}{\partial t} = \operatorname{div}(\mathbf{W}) = \lim_{\Delta V \to 0} \frac{\Delta s \dfrac{\partial}{\partial s}\left((2\pi r \sin\theta \Delta n W) + \Delta n \dfrac{\partial}{\partial n}(2\pi r \sin\theta \Delta s \rho) U\right)}{2\pi r \sin\theta \, \mathrm{d}s \, \mathrm{d}n} , \tag{5.1}$$

where ds and dn are differential line elements in the directions of the streamline and of its normal, respectively, $\mathbf{r}$ is the solar distance, θ the angle between the radius vector $\mathbf{r}$ and the upwind direction, and $\mathbf{W} = \rho \cdot \mathbf{v}$ is the local flow vector. This expression can be evaluated for the stationary case and yields:

$$\frac{\partial}{\partial s} \ln W + \frac{\sin \omega}{r \sin \theta} - \frac{\partial \omega}{\partial n} = \pm \frac{K(s)}{W} \left[\frac{1}{Z} + \frac{\partial \omega}{\partial n} - \frac{\cos \omega}{r \sin \theta} \right]. \tag{5.2}$$

Here the angle ω denotes the inclination between the local flow vector $\mathbf{W}$ and the upwind direction. $K = K(s) = \rho U$ is the diffusion flow perpendicular to the streamline which is a function of the line element ds. Expression (5.2) can be evaluated at the heliopause where $R_{\mathrm{HP}} = R_{\mathrm{HP}}(\theta)$. This is then used to give the change of the streamline inclination normal to the heliopause by:

$$\left| \frac{\partial \omega}{\partial n} \right|_{\mathrm{HP}} = \left| \frac{\dfrac{\partial}{\partial s} \ln W + \dfrac{\sin \omega}{R_{\mathrm{HP}} \sin \theta} (1 \pm \overline{K}(s) \operatorname{cotg} \omega) \pm \dfrac{\overline{K}(s)}{Z}}{1 \pm \overline{K}(s)} \right|_{\mathrm{HP}}. \tag{5.3}$$

Here the quantity $\overline{K}(s)$ denotes the local diffusive flow normalized with the magnitude of the main flow vector $\mathbf{W}(s)$. In this formula, the gradient of K was approximated by the diffusive flow across the heliopause divided by the extent Z of the heliopause boundary. If ω_0 is considered as the local inclination of the heliopause resulting for $K = 0$, one can derive the following expression for the change of the local inclination angle over the dimension Z of the heliopause layer due to K being nonzero.

$$\Delta\omega|_{\mathrm{HP}} \simeq Z \left| \frac{\partial}{\partial n} \mathrm{d}\omega \right|_{\mathrm{HP}} = \frac{\overline{K}}{1 \pm \overline{K}} \times$$

$$\times \left(1 \pm \frac{Z}{R_{\mathrm{H}}} \frac{\cos \omega}{\sin \theta} \pm \frac{Z \dfrac{\partial \ln W}{\partial s} + \dfrac{Z}{R} \dfrac{\sin \omega}{\sin \theta} (1 \pm \overline{K} \operatorname{cotg} \omega \pm \overline{K})}{(1 \pm \overline{K})} \right) \tag{5.4}$$

If in this formula only the linear terms in $\overline{K}$ are kept, one obtains:

$$\Delta\omega|_{\mathrm{HP}} = \overline{K} \left(1 \pm Z \frac{\partial \ln W}{\partial s} \right) \simeq \overline{K} \left(1 \pm \frac{Z}{\dfrac{\pi}{2} R_{\mathrm{HP}}} \right) \simeq \overline{K}, \tag{5.5}$$

where R_{HP} is the solar distance of the heliopause, which is considered to be very large in comparison to Z. In this formula, it becomes evident how important knowledge about possible mixing or diffusion processes across the heliopause is with concern to a consistent calculation of the resulting heliopause configuration. Equation (5.5) can be

interpreted as saying that for a main plasma diffusion flow K into the heliosphere, a cylindrical heliopause with a cone angle of $\mathrm{tg}\,\alpha \simeq \overline{\Delta\omega}|_{\mathrm{HP}} = \overline{K}$ can be expected.

Another aspect that is worth mentioning is the influence of the external flow on the side 1 flow lines. As the 'side 2' plasma is much denser than the 'side 1' plasma, the latter will rather easily adjust its speed to the tangential velocity of the plasma entering the heliosphere. One can expect immediate effects of this type up to the depth of penetration of external plasma. In addition, if the magnetic field in the shocked solar wind layer has a significant component in the radial direction, one might also expect interesting effects due to the 'projection' of the $(\mathbf{U}_2 - \mathbf{U}_1) \times \mathbf{B}_1$ electric fields. Such a 'projection' might lead to $\mathbf{E} \times \mathbf{B}$ drifts of the entire side 1 plasma, in accordance with the motion of the dense external plasma. Such a dynamic effect cannot be excluded since the Alfvén speed in medium 1 is higher than the expected tangential velocity difference $|\mathbf{U}_1 - \mathbf{U}_2|$, at least in the vicinity of the 'nose' (cf. Table I). In the case of strong coupling, the whole structure of side 1 might be substantially changed and, hence, the 'downwind' conditions of the terminating shock in the solar wind, including a shift in its location.

6. Conclusions: Plasma Mixing Across the Heliopause and Its Observational Implications

6.1. General facts

The most important conclusion which may be drawn from our investigations in Sections 2 through 4 is that the heliopause cannot be considered as a clearly defined surface separating the LISM plasma from the shocked solar wind flow. Rather, it has to be treated as a more or less extended transition layer with stationary or turbulent plasma properties, depending on the specific plasma conditions at the interstellar side. A substantial rate of plasma mixing is likely to take place across this transition layer. The physical basis of this plasma transport is different for the different LISM plasma signatures and also may change with time due to variations in the solar wind plasma conditions during the solar activity cycle.

If the LISM magnetic field is weak (below 10^{-7} G), the width of the transition region is likely to be determined by hydrodynamical Rayleigh–Taylor and Kelvin–Helmholtz instabilities developing in the adjacent plasma flows. As was discussed in Section 2 of this paper, the latter is likely to be the dominant instability mode. The extent of the highly turbulent transition region could then easily amount to 10 AU. As was discussed in Section 5.1, the contribution to the turbulent structure of this plasma in the transition layer by Rayleigh–Taylor instabilities would be spatially limited to the nose region of the heliopause and temporarily restricted to specific phases of the solar cycle when the heliopause is perturbed by a fast increase of the solar wind plasma pressure.

In the opposite case of strong LISM magnetic fields of the order of 10^{-6} G or more (possibly more realistic), the structure of the heliopause is expected to be fairly different, and most likely comparable to either the case of the distant planetary magnetopauses or to a typical plasma sheath in front of a wall. The similarity of the heliopause to the

distant tail of planetary magnetopauses with plasma transfer determined by reconnection processes will be stressed if the outside LISM magnetic field offers an appropriate component normal to the heliopause boundary surface. If, in contrast, the outside field is mainly tangential and also points into the direction of the solar wind magnetic field, reconnection is fairly unlikely and ineffective with respect to plasma transport. Under these conditions, the heliopause should be a transition layer with a width of some ten local ion gyroradii and plasma diffusion driven by electrostatic instabilities and ranging up to the order of the thermal mass flow at the side of the more tenuous plasma, i.e., the solar wind plasma.

Though a broad variety of heliopause transition layer structures is possible, depending on the different LISM plasma conditions, a common fact in all cases is a plasma transport across the heliopause. Thus the plasma- and field-transmission properties of the heliopause have to be taken into account in future investigations of heliopause-related phenomena. In the succeeding paragraphs we shall, therefore, discuss some of the observational implications of the 'leaky' heliopause.

6.2. Related Phenomena

6.2.1. *Location of the Heliopause*

In the case of a stable heliopause layer, its location, i.e., the solar stand-off distance, will depend on whether or not this layer is 'leaky'. If it is 'leaky' or semipermeable, some fraction of the impinging LISM plasma flow is transmitted through the heliopause. Thus only a part P'_{20} of the total LISM plasma pressure P_{20} has to be equilibrated by the solar wind counteraction. To estimate the corresponding reaction of the heliopause location to this change in pressure, we may use the subsonic plasma–plasma interface model given by Parker (1963). In this model, the stand-off distance L of the stagnation point from the Sun is determined by:

$$L^2 = \frac{1}{2}\sqrt{\frac{\rho_E U_E}{\rho_{2\infty} U_{2\infty}}}\sqrt{\frac{\rho_E U_E^2}{K(M_1, \gamma_1) P_{20}}}. \tag{6.1}$$

Here the function $K(M_1, \gamma_1)$ is the so-called pressure adaptation function given by Fahr *et al.* (1978) in the form:

$$K(\overline{M}_1, \overline{\gamma}_1) = \frac{\overline{\gamma}_1(\overline{\gamma}_1 + 1)\overline{M}_1}{2\overline{\gamma}_1\overline{M}_1^2 - (\overline{\gamma}_1 - 1)}\left[\frac{(\overline{\gamma}_1 + 1)^2\overline{M}_1^2}{4\overline{\gamma}_1\overline{M}_1^2 - 2(\overline{\gamma}_1 - 1)}\right]^{-\overline{\gamma}_1/(\overline{\gamma}_1 - 1)}, \tag{6.2}$$

where $\overline{M}_1$ and $\overline{\gamma}_1$ are the local sonic Mach number and the polytropic index of the pre-shock solar wind plasma at the heliospheric shock. The subscripts '2_∞' and 'E' denote the corresponding quantities of the unperturbed LISM and of the solar wind plasma at earth orbit, respectively. The LISM stagnation pressure P_{20} in the case of a non-transmissive heliopause is related to the unperturbed LISM plasma properties by:

$$P_{20} = \frac{1}{2}\frac{\gamma_2 - 1}{\gamma_2}\rho_{2\infty} U_{2\infty} + P_{2\infty}, \tag{6.3}$$

where γ_2 is the polytropic index of the LISM plasma. However, if the heliopause has a specific leakage rate $K = \rho_2 U_z \simeq \rho_{2\infty} c_{2\infty}$ with $c_{2\infty}$ as the sound velocity of the unperturbed LISM plasma, this plasma pressure would reduce to

$$P'_{20} = P_{20} - KU_z \simeq P_{20} - \rho_{2\infty} C^2_{2\infty} . \tag{6.4}$$

From Equations (6.1), (6.3), and (6.4), one may derive the following ratio between the stand-off distances L' and L of the transmissive and the non-transmissive heliopause, respectively:

$$(L'/L) = \sqrt[4]{P_{20}/P'_{20}} = \sqrt[4]{1 - \rho_{2\infty} C^2_{2\infty}/P_{20}} . \tag{6.5}$$

Adopting a value of 0.3 for the ratio $\rho_{2\infty} c_{2\infty}/P_{20}$, one obtains from (6.5) that the stand-off distance L' of the transmissive heliopause is larger by about 10% compared to L. This corresponds to a shift of the heliopause location by $\Delta L = L' - L \simeq 20$ AU, if L is assumed to be 210 AU.

6.2.2. *Penetration of Neutral LISM Particles into the Heliosphere*

As was demonstrated by Ripken and Fahr (1983) and Fahr and Ripken (1984), the probability of penetration of LISM neutral atoms, especially H and O, into the heliosphere, strongly depends on the structure of the plasma interface between the two regions. Depending on the proton density $\rho_{2\infty}$ and the stagnation pressure P_{20} of the LISM for those species, a variable density reduction occurs until they reach the heliopause. This reduction is caused by net charge exchange losses from the primary gas flow into secondary flow vectors of the perturbed LISM ion plasma. Ripken and Fahr (1983) have calculated the reduction of the hydrogen atom density at the heliopause. With the most probable values for the LISM, they find a reduction factor EX_0 of about 0.5. If the plasma transmissitivity of the stable heliopause (strong LISM magnetic field) reduces the stagnation pressure by about 30%, the stand-off distance L is increased by 10% to L', the total plasma interface region is correspondingly blown up, and the extinction of neutral LISM H-atoms is changed by a factor that was recently given by Fahr and Ripken (1985):

$$n_{\mathrm{H}}(L') = n_{\mathrm{H},\infty}(EX_0)^{(L'/L)} = n_{\mathrm{H},\infty}(EX_0)^{1.1} . \tag{6.6}$$

With a value of $EX_0 = 0.5$, we would arrive at an extinction factor $EX'_0 = 0.47$, i.e., a slightly higher extinction in the case of a transmissive heliopause.

This change in the neutral LISM extinction factor does not appear to be very spectacular since the absolute values of the unperturbed LISM density are not precisely known. However, one could imagine a temporal variability of this quantity by the order of 10% due to changes in the heliopause transmissivities induced by solar activity variations. Since this effect would be closely connected with the solar wind magnetic field, it should be triggered by the 22-yr solar magnetic cycle.

The heliopause is likely to be unstable in the case of a weak LISM magnetic field due to both Rayleigh–Taylor instability modes in the nose region and to Kelvin–Helmholtz modes in the flank region. For well-developed MHD-turbulences of this type, one

expects a turbulent region of size λ_* of $\simeq 10$ AU for the main instability periods $\tau_* = \frac{1}{4}\tau_0$, where τ_0 is the solar activity period (see Section 2, Equation (2.1)). Therefore, the corresponding fluctuations in the transmissitivity of the LISM neutrals due to plasma turbulence in the heliospheric interface may be estimated by taking into account an interface with a dimension variable in time by ± 10 AU. The total variability amplitude thus corresponds to the modulating effect of $2\lambda_* = 20$ AU of turbulent interface plasma, yielding a fluctuation amplitude of the H-atom density at the heliopause given by:

$$dEX_0 = \exp(-2\lambda_* \rho_{2,\infty} \sigma_{ex} \bar{v}_{rel}/m_i U_{2,\infty}) = 0.9\,, \tag{6.7}$$

where the values of Table I have been used. The quantity σ_{ex} is the $H-H^+$ charge exchange cross section, which amounts to 1.5×10^{-15} cm^2 (Fahr and Ripken, 1984) for a mean relative velocity v_{rel} between LISM protons and H-atoms of 3×10^6 cm s^{-1}. A 10% density fluctuation of the H-atoms in the heliosphere thus could be expected as a consequence of the modulation by the turbulent interface plasma.

6.2.3. *Cosmic-Ray Propagation into the Heliosphere*

The high-energetic particle radiation detected within the heliosphere is found to be of different origins. Three main cosmic-ray components have been identified so far: the solar cosmic rays, the galactic cosmic rays, and the so-called anomalous component of the cosmic rays. It is claimed that the latter is connected with primary neutral LISM species that enter the heliosphere, become ionized there and, as secondary ions, are reaccelerated to high energies of about 10–20 MeV after being convected with the solar wind plasma flow towards the heliospheric shock (Fisk, 1976). Among these anomalous cosmic-ray particles, only ion species with first ionization potentials higher than 13.6 eV, like He, N, O, and Ne ions, have been found. These anomalous ions are likely to appear in a singly-ionized state, as was concluded by Cummings *et al.* (1984) from the study of the energy scaling rules governing the spectra of the different anomalous cosmic-ray species.

It is evident that only intensities and spectra of the galactic and perhaps of the anomalous cosmic-ray components are affected by the actual physical state and the temporal variability of the heliopause. The galactic cosmic-ray particles enter the solar system from outside the heliopause. Below some critical energy limit, their primary source spectrum is strongly modulated by pitch angle scattering, diffusion and convection processes in the frozen-in solar wind magnetic fields. The modulation strongly depends on the roughness, i.e., the fluctuation level, of the interplanetary field that determines the energy-dependent diffusion coefficient. This modulation is clearly shown to have a solar cycle periodicity (McDonald *et al.*, 1981). Disregarding this effect, it is quite evident that for the spectral intensity of the galactic cosmic-ray component, it is rather important whether the magnetic fields of the LISM are partially reconnected with the interplanetary fields.

If they are in fact reconnected, the chances of cosmic-ray particles to propagate from outside the solar system into the inner regions of the heliosphere should definitely be

better, at least for particle energies with corresponding gyroradii smaller than the typical sheath dimensions at the heliopause (about 10 AU). This means that cosmic-ray particles with energies below 100 MeV should vary in intensity, depending on the reconnection rate of the LISM fields with the interplanetary field, i.e., depending on the solar magnetic cycle.

The well-known 'solar cycle' cosmic-ray modulation is due to a long period variation of the interplanetary magnetic fluctuation level which causes a corresponding solar cycle variation of the diffusion coefficient. Whereas it has an influence varying with the energy, this new solar cycle effect on the galactic cosmic rays due to variations in the reconnecting areas at the heliopause causes an energy-independent variation of the spectral intensities. This should also be reflected in the anomalous cosmic-ray component if this were a radiation component with an extra-heliospheric origin.

If, however, it is true that the anomalous component of the cosmic rays is connected with primary LISM neutrals that become ionized in the heliosphere, it may not be directly influenced by the heliopause magnetic field structure. This influence may arise indirectly from solar cycle variations of the depletion factors for LISM neutrals penetrating through the plasma interface (see Section 6.2.2). Since this depletion is for example higher for hydrogen and oxygen and lower for helium and nitrogen, it follows that some solar cycle variations of the relative abundances of the anomalous cosmic-ray species should be observable.

6.2.4. *Generation of Radio Noise at the Heliopause*

The generation of different forms of electrostatic and electromagnetic waves at the heliopause can be expected because of the specific physical processes in this region. However, it is interesting to note that the type of waves predominantly generated there strongly depends on the specific structure of the heliopause layer. For instance, the type of heliopause layer discussed in Section 3 (with tangential magnetic fields mainly of equal polarity) is expected to produce electrostatic field turbulence excited by the double-peaked ion velocity distribution function. These radio waves could easily propagate into the tenuous solar wind plasma towards the inner heliosphere.

On the other hand, if strong magnetic fields of opposite polarity or an appreciable component in the normal direction to the heliopause occur, a transition layer determined by magnetic field reconnection processes would result. Galeev and Sagdeev (1984) then predict that electrostatic waves, typically at the lower hybrid frequency $\omega_{lh} = \sqrt{\omega_{ge}\omega_{gi}}$ will be generated for standard reconnection models. These waves propagate only into directions strictly perpendicular to the local magnetic fields and quickly die out in other directions.

For a heliopause with small magnetic fields ($\leq 10^{-7}$ G), only macroscopic turbulence of the Rayleigh–Taylor and Kelvin–Helmholtz types is expected. These cannot be considered as candidates for radio noise generators in the propagation branch of frequencies.

Since electron and ion densities n_2 of about 2×10^{-2} cm^{-3} can be expected at the interstellar side, the two stream ionflow situation in the heliopause layer is likely to

coexist with a statistical level of electrostatic radio noise at frequencies of $\nu_{pe} = \omega_{pe}/2\pi = 1273\,\text{Hz} \simeq 1.3\,\text{kHz}$ for an electrostatically turbulent heliopause layer. This radio noise could propagate freely into the region of the tenuous solar wind plasma towards the inner heliosphere, and finally die out at a solar distance of $r < r_c$, where the local plasma frequency becomes larger than the radio noise frequency, i.e., at:

$$r_c/r_E = \sqrt{n_E/n_2} = 15.8\,. \tag{6.8}$$

In this context, it is interesting to recall that recently electrostatic radio noise in the frequency range between 1.3 and 1.8 kHz was recorded by plasma wave receivers on Voyager 1 and 2 at solar distances beyond 13 AU (Kurth *et al.*, 1984). However, these radio emissions were ascribed by these authors to emissions from the heliospheric shock front at twice the plasma frequency. This is attributed to a heliospheric shock front at 46 AU.

It is hard to believe that the heliospheric shock front is located so close to the Sun, since all theoretical investigations lead to a much larger distance of about 100 AU (see, e.g., Axford, 1972; Fahr *et al.*, 1978; Baranov *et al.*, 1979; Ripken and Fahr, 1983). We are, therefore, suggesting here an alternative possibility to explain these radio emissions to be electrostatic plasma waves originating *at the heliopause*. An interesting fact is that the interplanetary radio emission near 3 kHz was observed by Kurth *et al.* (1984) only during phases of low cosmic ray proton count rates (3–17 MeV protons), i.e., at quiet interplanetary conditions, as was recognized by Lanzerotti *et al.* (1985). However, this fact could possibly be interpreted in a very different way: radio wave emissions of this kind are perhaps emitted from the heliopause only during phases when the local magnetic field conditions are favourable for the generation of electrostatic plasma turbulence, i.e., at specific phases of the solar cycle.

References

Akasofu, S. I. and Covey, D. N.: 1981, *Planetary Space Sci.* **29**, 313.

Axford, W. I.: 1972, *Solar Wind II*, NASA SPR-308.

Bame, S. J., Anderson, R. C., Asbridge, J. R., Baker, D. N., Feldman, W. C., Gosling, J. T., Hones, E. W. Jr., McComas, D. J., and Zwickl, R. D.: 1983, *Geophys. Res. Letters* **10**, 912.

Baranov, V. B., Krasnobaev, K. V., and Ruderman, M. S.: 1976, *Astrophys. Space Sci.* **41**, 491.

Baranov, V. B., Lebedev, M. G., and Ruderman, M. S.: 1979, *Astrophys. Space Sci.* **66**, 441.

Berchem, J. and Russell, C. T.: 1984, *J. Geophys. Res.* **89**, 6689.

Bertaux, J. L.: 1984, in Y. Kondo, F. C. Bruhweiler, and B. D. Savage (eds.), 'Local Interstellar Medium', *IAU Colloq.* **81**, 3.

Braginski, S. I.: 1957, *Soviet Phys.* **6**, 358.

Burlaga, L. F.: 1984, *Space Sci. Rev.* **39**, 255.

Burlaga, L. F., Klein, L. W., Lepping, R. P., and Behannon, K. W.: 1984, *J. Geophys. Res.* **89**, 10659.

Burlaga, L. F., Lepping, R. P., Behannon, K. W., Klein, L. W., and Neubauer, F. M.: 1982, *J. Geophys. Res.* **87**, 4345.

Burlaga, L. F., Schwenn, R., and Rosenbauer, H.: 1983, *Geophys. Res. Letters* **10**, 413.

Chandrasekhar, S.: 1961, *Hydrodynamic and Hydromagnetic Stability*, Dover Publ. Inc., New York.

Coleman, P. J., Jr.: 1976, in E. W. Greenstadt, M. Dryer, and D. S. Intriligator (eds.), *Exploration of the Outer Solar System*, American Institute of Aeronautics and Astronautics, New York, p. 3.

Cowley, S. W. H.: 1982, *Rev. Geophys. Space Phys.* **20**, 531.

Crooker, N. U.: 1979, *J. Geophys. Res.* **84**, 951.

Crooker, N. U.: 1982, *Solar Wind V*, Proc. Conf. Woodstock, Vermont, p. 303.
Cummings, A. C., Stone, E. C., and Webber, W. R.: 1984, *Astrophys. J.* **287**, L99.
Davidson, L. R.: 1984, in A. A. Galeev and R. Sudan (eds.), *Osnovy Fiziki Plasmy*, Vol. 1, Energoatomizdat, Moscow, p. 443.
Davidson, R. C., Krall, N. A., Papadopoulos, I., and Shanny, R.: 1969, *Phys. Rev. Letters* **24**, 579.
Fahr, H. J. and Neutsch, W.: 1982a, *Astron. Astrophys.* **118**, 57.
Fahr, H. J. and Neutsch, W.: 1982b, *Monthly Notices Roy. Astron. Soc.* **205**, 839.
Fahr, H. J. and Ripken, H. W.: 1984, *Astron. Astrophys.* **139**, 551.
Fahr, H. J. and Ripken, H. W.: 1985, 'The Heliospheric Plasma Interface for Different LISM Phases', *Astron. Astrophys.* (submitted).
Fahr, H. J., Grzedzielski, S., and Ratkiewicz-Landowska, R.: 1985, in preparation.
Fahr, H. J., Petelski, E. F., and Ripken, H. W.: 1978, *Solar Wind IV*, NASA-SPR W-100-81-31, 543.
Fejer, J. A.: 1964, *J. Geophys. Res.* **69**, 123.
Fejer, J. A.: 1965, *J. Geophys. Res.* **70**, 4972.
Feldman, W. C.: 1981, *Solar Wind IV*, Proc. Burghausen, Springer-Verlag, Berlin, Heidelberg, New York, p. 217.
Feldman, W. C., Asbridge, J. R., Bame, S. J., Fenimore, E. E., and Gosling, J. T.: 1981, *J. Geophys. Res.* **86**, 5408.
Fisk, L. A.: 1976, *J. Geophys. Res.* **81**, 4646.
Galeev, A. A.: 1978, *Phys. Fluids* **21**, 1353.
Galeev, A. A.: 1983, *Space Sci. Rev.* **34**, 213.
Galeev, A. A. and Sagdeev, R.: 1984, in A. A. Galeev and R. Sudan (eds.), *Osnovy Fiziki Plasmy*, Complement to Vol. 2, Energoatomizdat, Moscow, 1984, p. 5.
Gladd, N. T. and Horton, W., Jr.: 1973, *Phys. Fluids* **16**, 879.
Grzedzielski, S. and Macek, W.: 1984, *J. Geophys. Res.* **89**, 2369.
Grzedzielski, S., Macek, W., and Ziemkiewicz, J.: 1986, to appear.
Grzedzielski, S., Macek, W., and Oberc, P.: 1981, *Nature* **292**, 615.
Grzedzielski, S., Macek, W., and Oberc, P.: 1982, *Astra Astron.* **32**, 309.
Heyn, M. F., Biernat, K., Semenov, V. S., and Kubyshkin, I. V.: 1985, *J. Geophys. Res.* **90**, 1781.
Horton, V.: 1984, in A. A. Galeev and R. Sudan (eds.), *Osnovy Fiziki Plasmy, Vol. 2, Energoatomizdat*, 1984, p. 363.
Hundhausen, A. J.: 1979, *Rev. Geophys. Space Phys.* **17**, 2034.
Kadomtsev, B. B.: 1965, *Plasma Turbulence*, Academic Press, New York.
Kayser, S. E., Barnes, A., and Mihalov, J. O.: 1984, *Astrophys. J.* **285**, 339.
Kurth, W. S., Gurnett, D. A., Scarf, F. W., and Poynter, R. L.: 1984, *Nature* **312**, 27.
Kurth, W. S., Sullivan, J. D., Gurnett, D. A., Scarf, F. L., Bridge, H. S., and Sittler, E. C., Jr.: 1982, *J. Geophys. Res.* **87**, 10373.
Landau, L. D. and Lifshitz, E. M.: 1963, *Electrodynamics of Continuous Media*, Pergamon Press, Oxford, Chapter VIII.
Lanzerotti, L. J. and Maclennan, C. G.: 1985, *Nature* **316**, 243.
Lee, L. C.: 1982, *Geophys. Res. Letters* **9**, 1159.
Lee, L. C. and Roederer, J. G.: 1982, *J. Geophys. Res.* **87**, 1439.
Lepping, R. P., Burlaga, L. F., Desch, M. D., and Klein, L. W.: 1982, *Geophys. Res. Letters* **9**, 885.
Lerche, I.: 1966, *J. Geophys. Res.* **71**, 2365.
Liu, C. S., Rosenbluth, M. N., and Horton, C. W., Jr.: 1972, *Phys. Rev. Letters* **29**, 1489.
Luhmann, J. G., Walker, R. J., Russell, C. T., Crooker, N. U., Spreiter, J. R., and Stahara, S. S.: 1984a, *J. Geophys. Res.* **89**, 1739.
Luhmann, J. G., Walker, R. J., Russell, C. T., Spreiter, J. R., Stahara, S. S., and Williams, D. J.: 1984b, *J. Geophys. Res.* **89**, 6829.
Macek, W. and Grzedzielski, S.: 1984, in B. McNamara (ed.), 'Radiation in Plasmas', *Proc. Int. Centre Theoret. Phys., Trieste*, Vol. 2, p. 706, World Scientific, Philadelphia, Singapore.
Macek, W. and Grzedzielski, S.: 1985, in B. McNamara (ed.), *Twenty Years of Plasma Physics*, World Scientific, Philadelphia, p. 320.
Macek, W. and Grzedzielski, S.: 1986, in W. Grossman (ed.), *Proc. Int. Centre Theoret. Phys., Trieste* (in press).
McDonald, F. B., Lal, N., Trainor, J. H., Van Hollebeke, M. A. I., and Webber, W. R.: 1981, *Astrophys. J.* **249**, L71.

Miura, A.: 1982, *Phys. Rev. Letters* **49**, 779.
Miura, A.: 1984, *J. Geophys. Res.* **89**, 801.
Miura, A., and Pritchett, P. L.: 1982, *J. Geophys. Res.* **87**, 7431.
Neutsch, W. and Fahr, H. J.: 1983, *Monthly Notices Roy. Astron. Soc.* **202**, 735.
Olson, W. P. and Pfitzer, K. A.: 1984, *J. Geophys. Res.* **89**, 7347.
Papadopoulos, K.: 1977, *Rev. Geophys. Space Phys.* **15**, 113.
Parker, E. N.: 1958, *Phys. Fluids* **1**, 171.
Parker, E. N.: 1963, in *Interplanetary Dynamical Processes*, Interscience, New York.
Parker, E. N.: 1967a, *J. Geophys. Res.* **72**, 2315.
Parker, E. N.: 1967b, *J. Geophys. Res.* **72**, 4365.
Parker, E. N.: 1977, *Astrophys. J.* **215**, 370.
Parker, E. N.: 1979, *Cosmical Magnetic Fields*, Clarendon Press, Oxford, p. 392ff.
Paschmann, G., Sonnerup, B. U. Ö., Papamastorakis, I., Sckopke, N., Haerendel, G., Bame, S. J., Asbridge, J. B., Gosling, J. T., Russell, C. T., and Elphic, R. C.: 1979, *Nature* **282**, 243.
Pilipp, W. G.: 1983, *Solar Wind V*, NASA SPR-2280, p. 413.
Ratkiewicz-Landowska, R. and Grzedzielski, S.: 1984, *Artif. Satell.* **19**, No. 2.
Ratkiewicz-Landowska, R., Fahr, H. J., and Grzedzielski, S.: 1985, in preparation.
Ripken, H. W. and Fahr, H. J.: 1983, *Astron. Astrophys.* **122**, 181.
Robertson, C., Cowley, S. W. H., and Dungey, J. W.: 1981, *Planetary Space Sci.* **29**, 399.
Russell, C. T. and Elphic, R. C.: 1979, *Geophys. Res. Letters* **6**, 33.
Schlüter, A.: 1950, *Z. Naturforsch.* **5**, 72.
Scudder, J.: 1984, *J. Geophys. Res.* **89**, 7431.
Sen, A. K.: 1965, *Planetary Space Sci.* **13**, 131.
Slavin, J. A., Tsurutani, B. T., Smith, E. J., Jones, D. E., and Sibeck, D. G.: 1983, *Geophys. Res. Letters* **10**, 973.
Smith, E. J. and Barnes, A.: 1982, *Solar Wind V*, Proc. of a Conference, Woodstock, Vermont, p. 521.
Smith, P. R.: 1984, *Planetary Space Sci.* **32**, 1147.
Smith, P. R., Cowley, S. W. H., and Dungey, J. W.: 1984, *Planetary Space Sci.* **32**, 1135.
Sonnerup, B. U. Ö.: 1970, *J. Plasma Phys.* **4**, 161.
Sonnerup, B. U. Ö. and Ledley, B. G.: 1974, *J. Geophys. Res.* **79**, 4309.
Sonnerup, B. U. Ö., Paschmann, G., Papamastorakis, I., Sckopke, N., Haerendel, G., Bame, S. J., Asbridge, J. R., Gosling, J. T., and Russell, C. T.: 1981, *J. Geophys. Res.* **86**, 10049.
Spitzer, L. 1956, *Physics of Fully Ionized Gases*, Interscience, New York.
Tange, T. and Ichimaru, S.: 1974, *J. Phys. Soc. Japan* **36**, 1437.
Tritakis, V. P.: 1984, *J. Geophys. Res.* **89**, 6588.
Vlasov, V. I.: 1983, *Geomagnetizm i Aeronomiya* **23**, 475.
Whittaker, E. T. and Watson, G. N.: 1927, *Modern Analysis*, Cambridge Univ. Press, Cambridge.
Willis, D. M.: 1971, *Rev. Geophys. Space Phys.* **9**, 953.
Winterhalter, D., Kivelson, M. G., Russell, C. T., and Smith, E. J.: 1981, *Geophys. Res. Letters* **8**, 911.